New three-dimensional network concept for deployable space antennas

William Bettini, Xavier Maetz, Jérôme Quirant, Julien Averseng, Bernard Maurin

New three-dimensional network concept for deployable space antennas

William Bettini [(a)], Xavier Maetz[(b)], Jérôme Quirant [(b)], Julien Averseng [(b)], Bernard Maurin [(b)]

Affiliations:

Bettini W., Associate Pr., LINEACT-CESI, La Canopée, 390 Rue Claude Nicolas Ledoux, 13290 Aix-en-Provence[(a)], France, wbettini@cesi.fr (corresponding author)

Maetz X., PhD Student, Laboratoire de Mécanique et Génie Civil (LMGC), Univ. Montpellier, CNRS, CC048, 163 rue Auguste Broussonnet, 34090 Montpellier[(b)], France, xavier.maetz@umontpellier.fr

Quirant J., Associate Pr., LMGC, Univ. Montpellier, CNRS, CC048, 163 rue Auguste Broussonnet, 34090 Montpellier, France, jerome.quirant@umontpellier.fr

Averseng J., Associate Pr., LMGC, Univ. Montpellier, CNRS, CC048, 163 rue Auguste Broussonnet, 34090 Montpellier, France, julien.averseng@umontpellier.fr

Maurin B., Professor, LMGC, Univ. Montpellier, CC048, 163 rue Auguste Broussonnet, 34090 Montpellier, CNRS, Montpellier, France, bernard.maurin@umontpellier.fr

Abstract

A new antenna design lighter, and with fewer mechanical connections between the elements has emerged. This concept consists of deploying a polygonal ring using the flexion energy present in the flexible joints connecting two consecutive bars. Shaped reflective surfaces can selectively avoid radiating to certain areas of the globe. However, these consist of rigid frames and are not deployable. Studies have been conducted to obtain a uniform tension in a mesh network. In order to tighten a shaped membrane into this new structure, a new type of network that can be inserted into the polygonal ring was studied. This new type of three-dimensional network that can fit into this ring or existing reflectors

has been developed with the aim of obtaining control points. Compared to the common cable domes used in civil engineering, the tension of this type of three-dimensional network is better distributed across all elements. Applications include shaped or meshed space antennas, and solar panel supports.

Keywords: three-dimensional network, space structure, antenna, cable dome, uniform tension.

I Introduction

Deployable space antennas consist of a frame into which a network of cables is inserted. In the literature, two major types of space antenna frame structures can be identified: peripheral ring skeleton like the Astromesh antenna (Fig. 1.a) and radiating frame structures like the TerreStar reflector (Fig. 1.b). On this network a meshed reflective surface rests. To design the network, many solutions exist and a solution based on tensegrity compatible with small satellites is proposed [1]. The peripheral ring is shaped by means of cable that creates a deformable parallelogram [2]. To minimize mechanisms, a self-deployable scissor-based and flexible joint based antenna concept has been developed at the LMGC [3]. The ring is directly prestressed thanks to the bending energy present in the flexible joints.

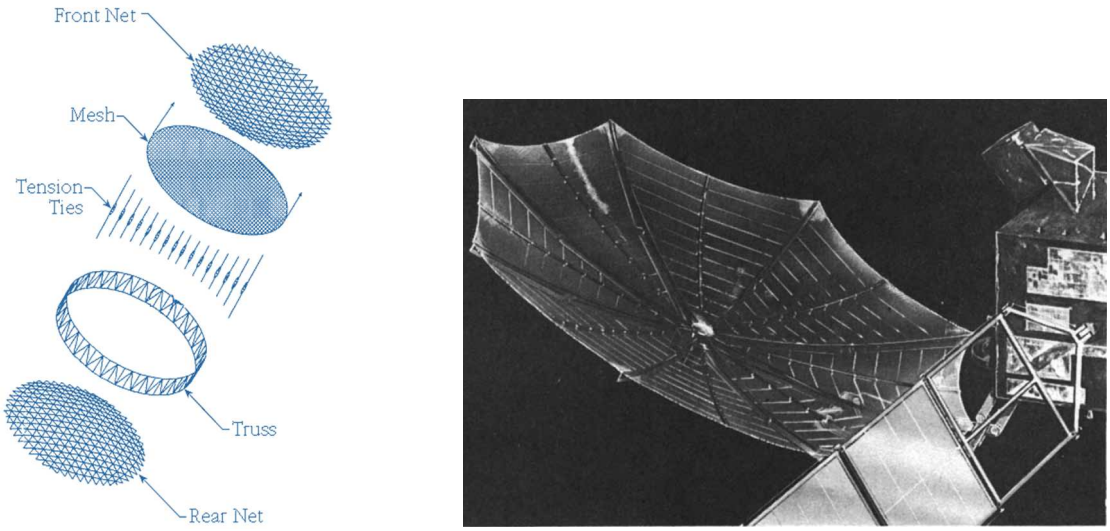

a. AstroMesh concept from Thomson 1997 [4] b. Terrestar reflector Kellermeier 1986 [5]

Fig. 1. Composition of a classic foldable antenna

The truss is foldable and shaped by cables. The rim tension the front net thanks to the network (Fig. 2).

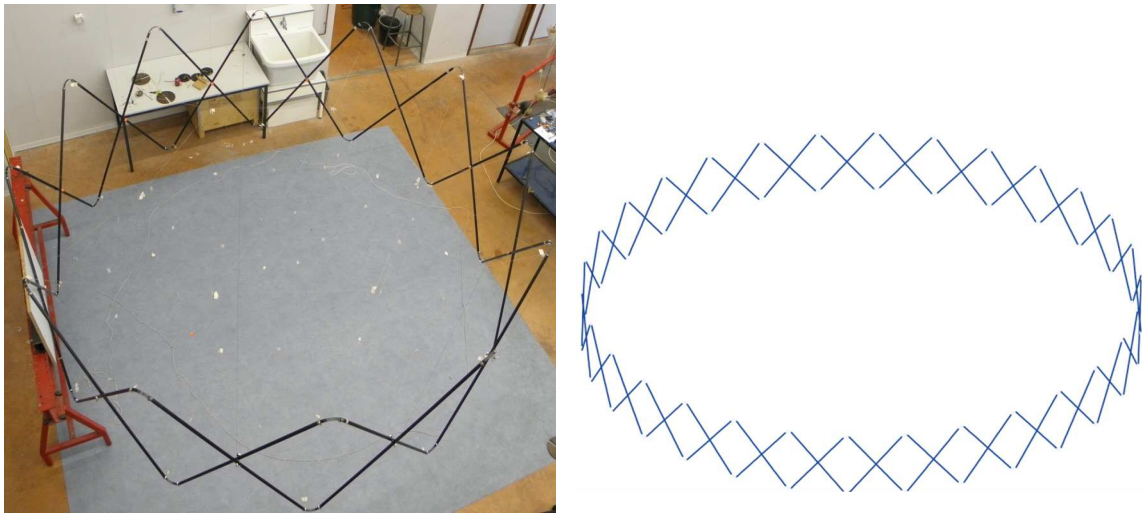

Fig. 2. Self deployable scissor based rim

A new, lighter, deployable ring, in which mechanical connections between elements are minimised by removing the scissors, was developed by Bettini [6]. This concept consists of deploying a polygonal ring that can either have a voluminous or flat final shape (Fig. 3.). This rim unfolds as described by Morterolle's [7], one using the flexion energy present in flexible joints connecting consecutively bars.

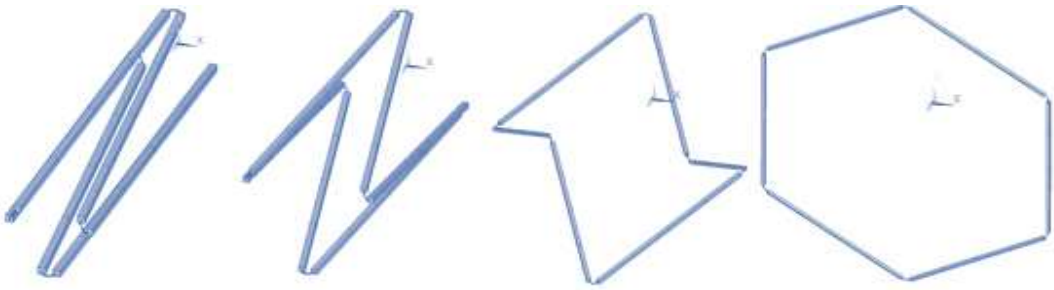

a b c d

Fig. 3. Different apertures of the peripheral ring (volumic a, b, c, and planar d)

Space antennas consist largely of a network of tensioned cables on which a reflective metallic mesh rests. In order to match at best a parabolic surface and obtain a better signal, uniform tension in a network is preferable [8, 9]. Another advantage of having a homogeneous distribution of tension on the cable net is a simpler effort of assembly and integration. As a result, a uniform tension algorithm was developed by Morterolle [8] for a cable network. However, these networks can only be used for surfaces whose geometry is a regular (not shaped) dish. The vast majority of space reflectors have a fixed and non-

modifiable reflective surface. Shaped surfaces return signals to a contoured area of the globe. A new concept in space antennas, similar to that of meshed antennas, has emerged; a peripheral ring extending a three-dimensional network composed of bars and cables on which comes to rest a membrane (Fig. 4.).

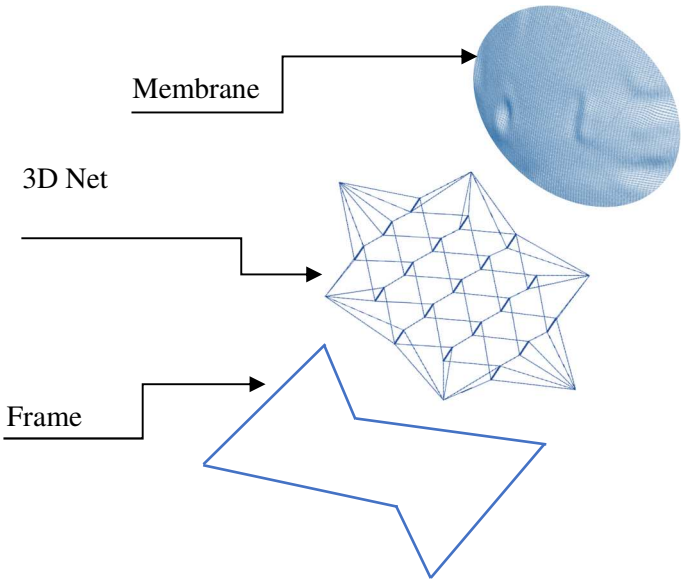

Fig. 4. Mesh antenna principle and new concept

This allows broadcasts on certain regions of the globe, restricting the transmission from certain areas of the reflective surface: it is a shaped surface. Cable domes provide rigid supports on which a membrane can rest. These supports can be adjusted (Fig. 5) to obtain a shape containing concave and convex regions (with negative double curvature).

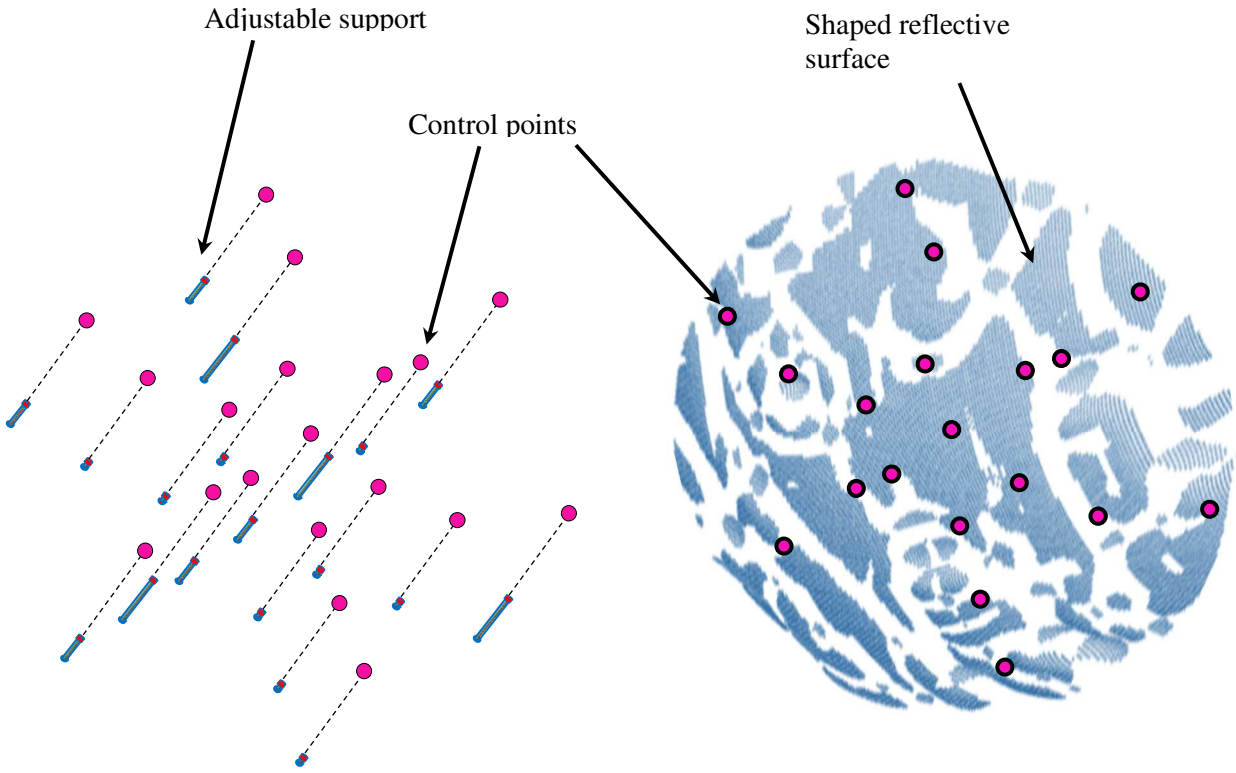

Fig. 5. Network with telescopic bars and shaped membrane

The reflector presented by Rodrigues [10] is mechanically deformable and reconfigurable. Its reflective surface is deformable thanks to actuators which exert pressure on the membrane at a targeted point. This type of reflector allows a large number of reconfigurations. Curves on the surface are often approximated by splines (polynomial function per piece). The surfaces used to form shaped surfaces can be implemented of CFRS (Carbon Fiber Reinforced Silicon). As described by [11], CFRS offers thermal, mechanical and reflexive capabilities useful for space applications. A study of the thermo-deformation of the CFRS surface is presented by Datashvili [12]. The disadvantage of Rodrigues's antenna is that it generates a considerable increase in antenna mass, which is not desirable in most cases.

Straight-wired domes from civil engineering are a solution to best approach a shaped reflective surface. Tensioned by means of a peripheral ring, control points are formed from the compressed bars. The most common cable domes are Fuller and Geiger (Fig. 6.). These three-dimensional networks were studied by Fayos [13] with a view to their application in the space domain.

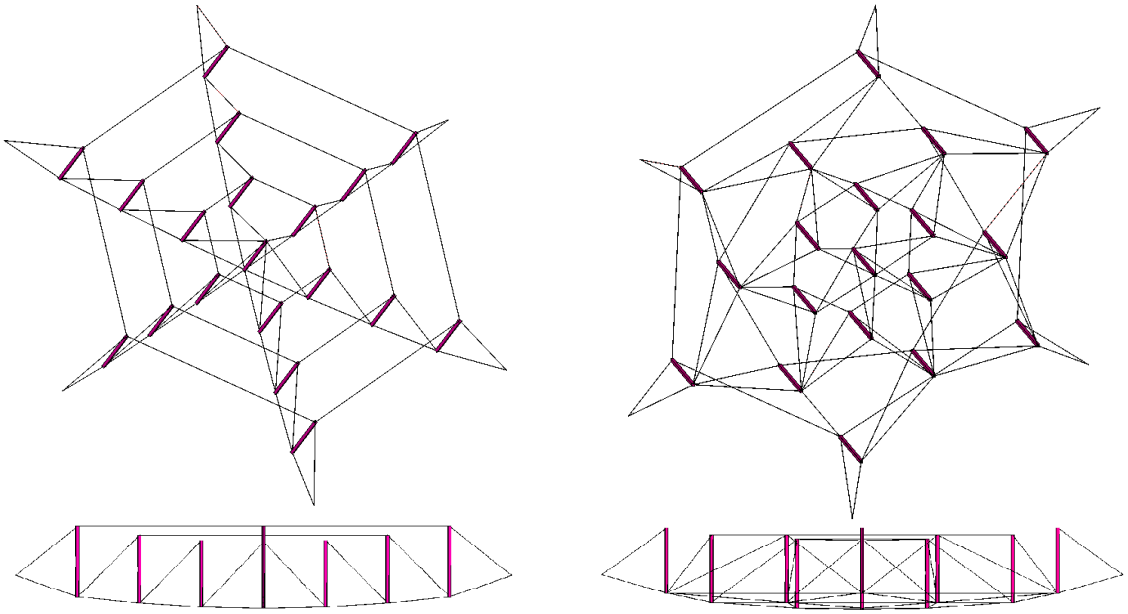

Fig. 6. Geiger and Fuller cable dome

Negative double curvature surfaces are often used on reflectors whose surface can be modulated using actuators. These actuators act as checkpoints. With the aim of applying this process to deployable space antennas, the LMGC has focused development of this type of surface with self-deployable peripheral rings. Of primary importance to the scaling of spatial structures are the stiffness of the skeleton in its deployed configuration, surface accuracy, stability and the form of the reflective surface in an operational configuration.

However, a problem with dome cables is the non-uniformity of tension. As explained by Fayos [14], the tension on the dome cable decreases markedly from to the periphery towards the center (Fig.7.).

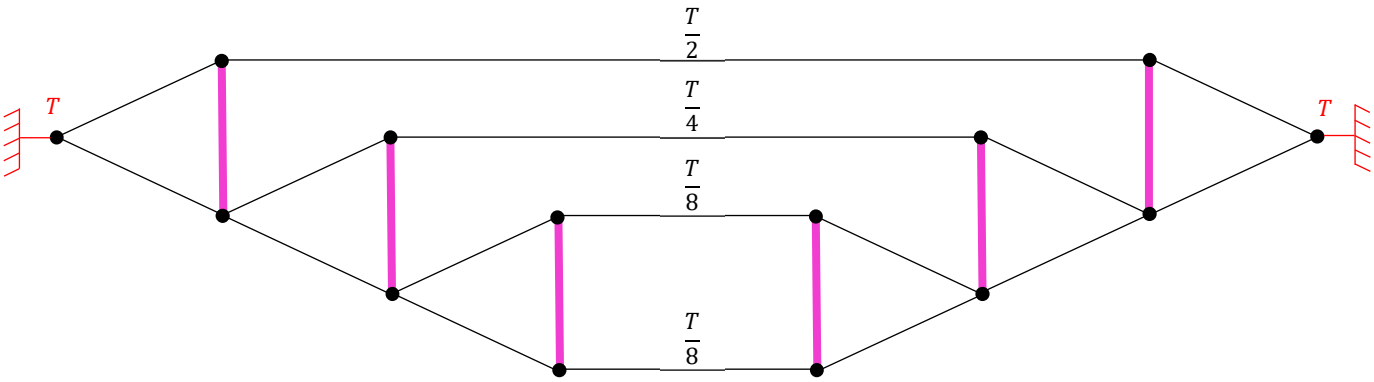

Fig. 7. Geiger cable dome (cutting plane)

Due to its low mass, the use of a cable-dome network is highly appreciated in the field of civil engineering for constructing roofs. Its curvature allows, among other things, for the drainage of rain water. The use of compressed bars allows for control points producing a topology containing concave and convex regions.

In this paper, static and modal analyses of a new kind of cable dome will be presented. The first part will describe the geometry of the new network while analytical models of the static analyses for further cable nets and their optimization are proposed in the second part. The third part deals with a mechanical study for a completed solution of a space antenna.

II Geometry and axial forces distribution of the new network

II.1 Geometry

One of the activities of the LMGC is the study of lightweight structures like tensegrity systems. These systems can be defined as reticulate, spatial, and in a stable state of selfstress. They include a discontinuous set of compressed elements and a continuous set of tensioned elements. Thus, the system is statically and cinematically undetermined. Statically, the selfstress state is defined with a multiplication factor a priori unknown. Cinematically some mechanisms can appear with infinitesimal strains in elements, stabilised by the selfstress [15].

The new dome configuration is inspired by Tensarch, a tensegrity grid elaborated by V. Raducanu, R. Motro in 2002 [16], made of an arrangement of bars, cables and tensioners (Fig.8).

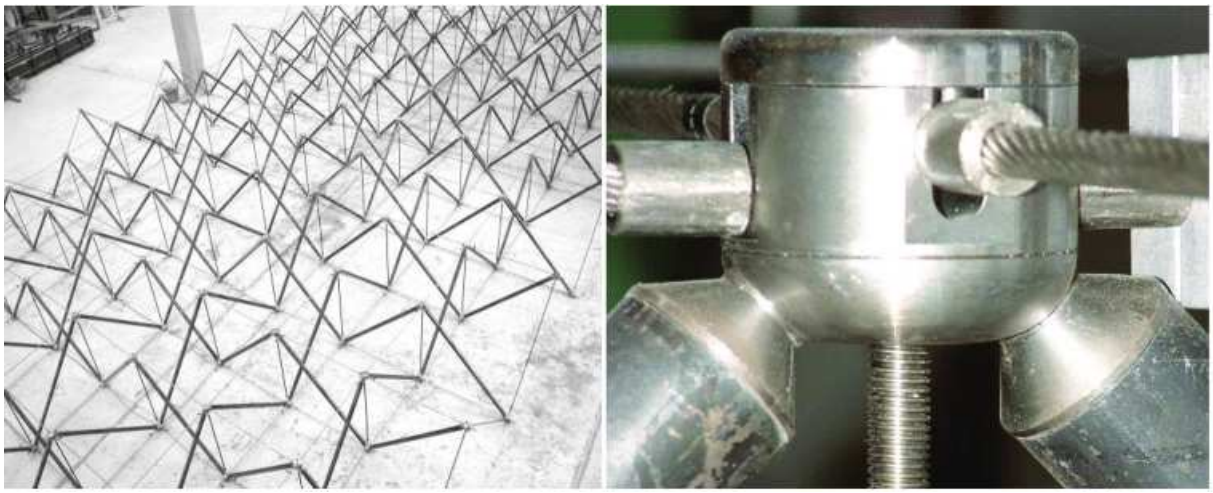

Fig. 8. Tensarch

In comparison, the principle behind the new proposal truss is that bars are replaced by cables, and tensioners become bars, lightening the structure and creating control points (Fig.9). Thus, the structure presents a three-direction network instead of two directions as seen in traditional Tensarch architecture. For this configuration, networks are stable with three cables per node for each bar, which results in pyramidal patterns.

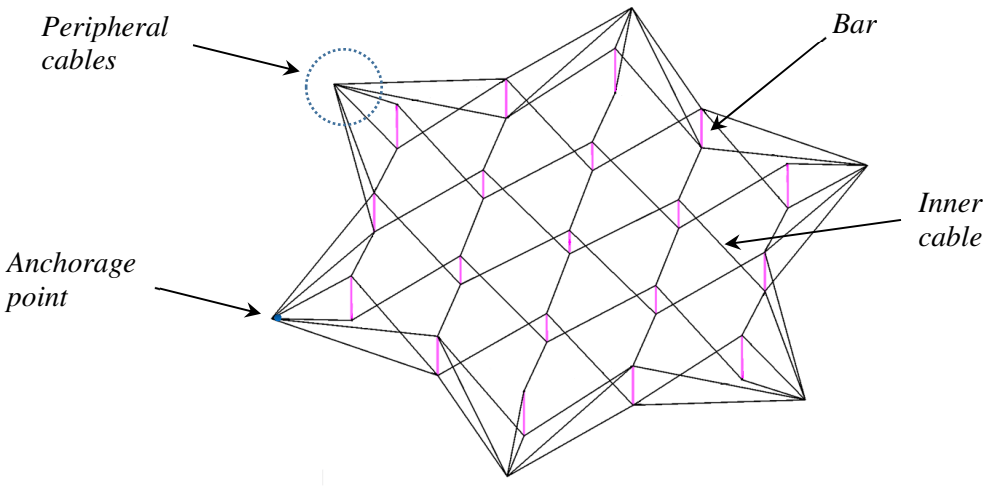

Fig. 9. Pyramidal network of 19 bars

For this type of network, two anchoring configurations have been modelled in order to obtain an optimal solution in terms of distribution of axial forces (Fig.10). It has been shown that the configuration (1) makes it possible to distribute the forces more evenly across the bars.

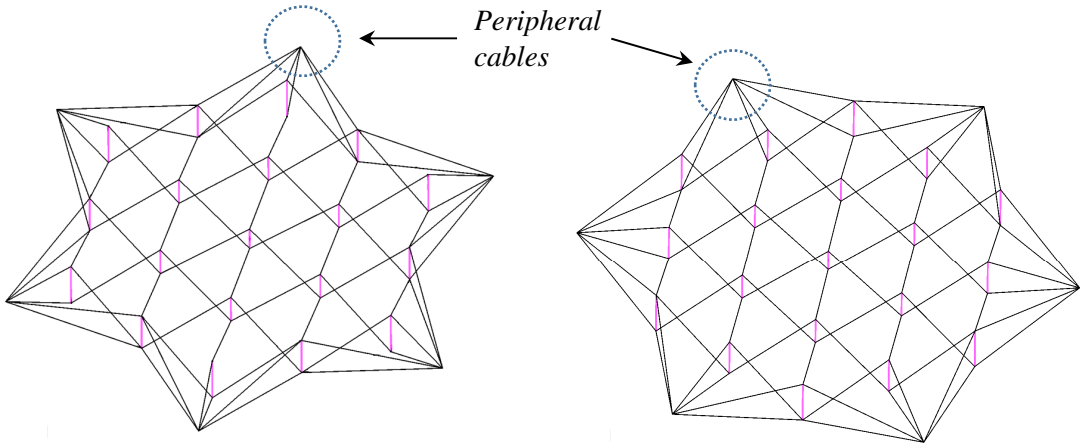

Configuration (1) Configuration (2)

Fig. 10. Different network anchorage configurations

This configuration can be tightened by a simple annular structure as shown in Figure 3. Figure 11 shows the assembly for a hexagonal ring with 6 attachment points on the beams of the ring. These attachment points are located in the centre of the ring bars and not at the ends for reasons of symmetry in the stowed configuration.

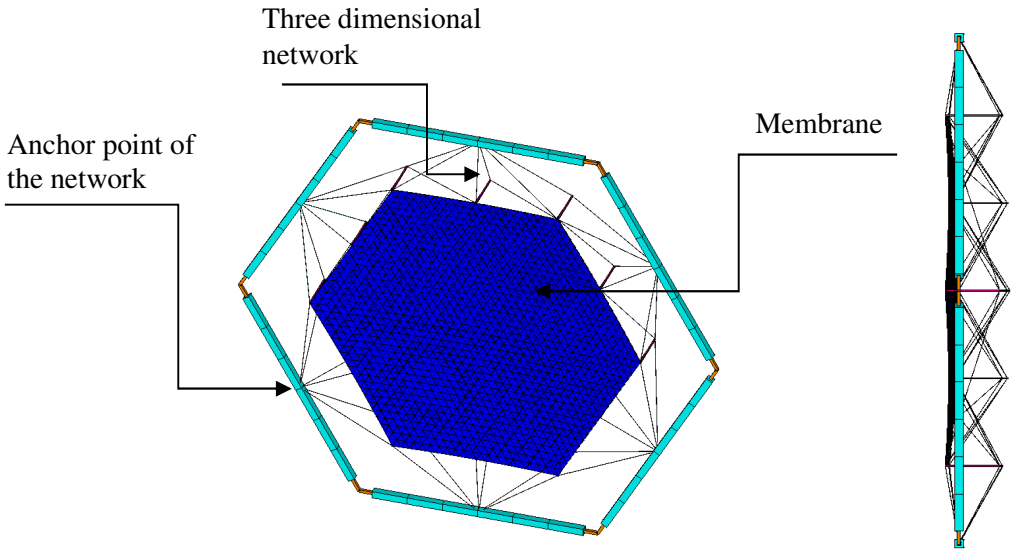

Fig. 11. A new concept for deployable antenna

Compared to existing structures such as the Astromesh, the useful surface is not equal to the area of the peripheral ring. The chosen rigging method (Fig. 12, Fig. 12 A) is not optimal for the folding process because the number of bars is equal to the number of rigging points, which means that the rigging must be connected at the centre of the bars. However, it is possible to double the number of bars (Fig. 12 C) in order to attach to nodes (upper or lower to allow stowing), which also minimises the torque generated on the joints by the network tension.

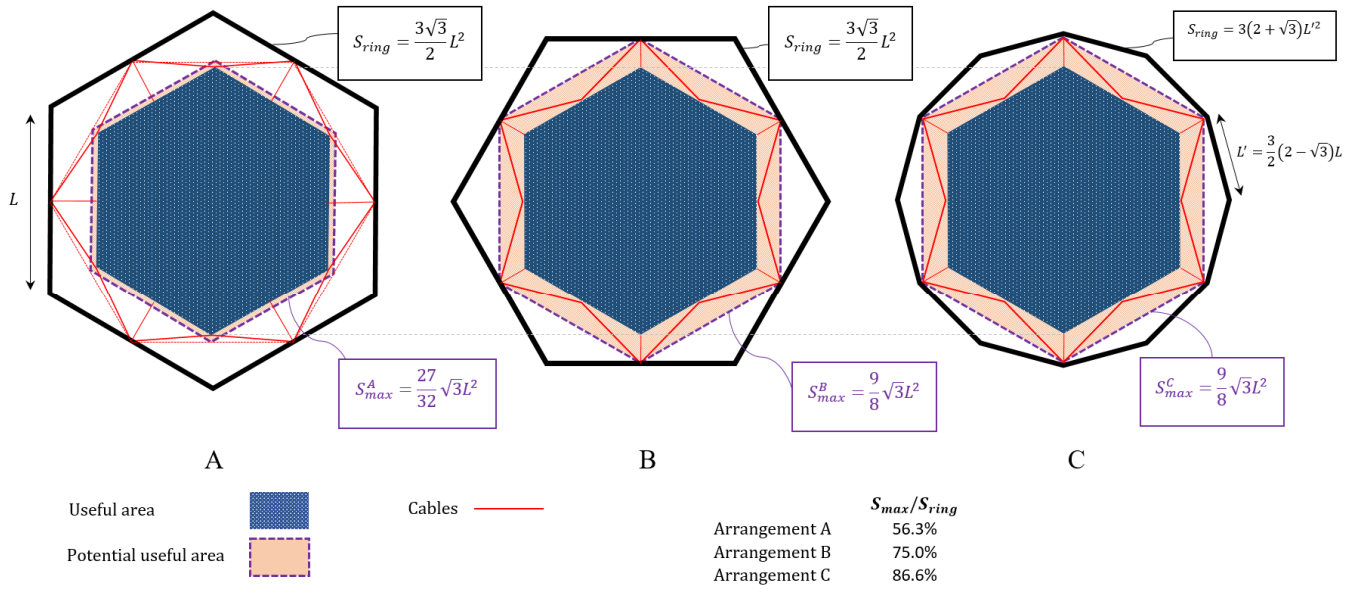

Fig. 12. Optimisation of the usable area

Another advantage of this new configuration is that each membrane attachment point is unobtrusive; there is no interference from the cables as in the Fuller and Geiger versions (Fig.13 top). The position of the cable net relative to the ring is adjustable, with the cable length and the depth of the parabola being obtained from the variation of the bar heights.

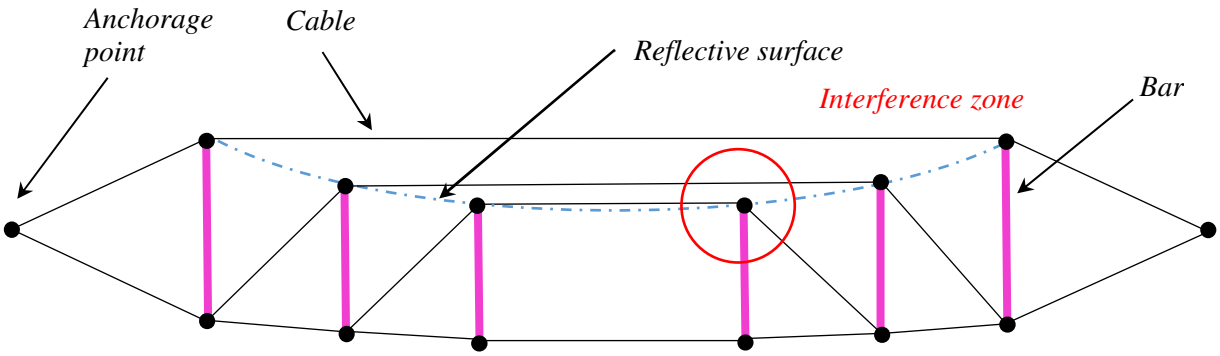

Interference with the membrane from a Geiger network (radial cutting plane)

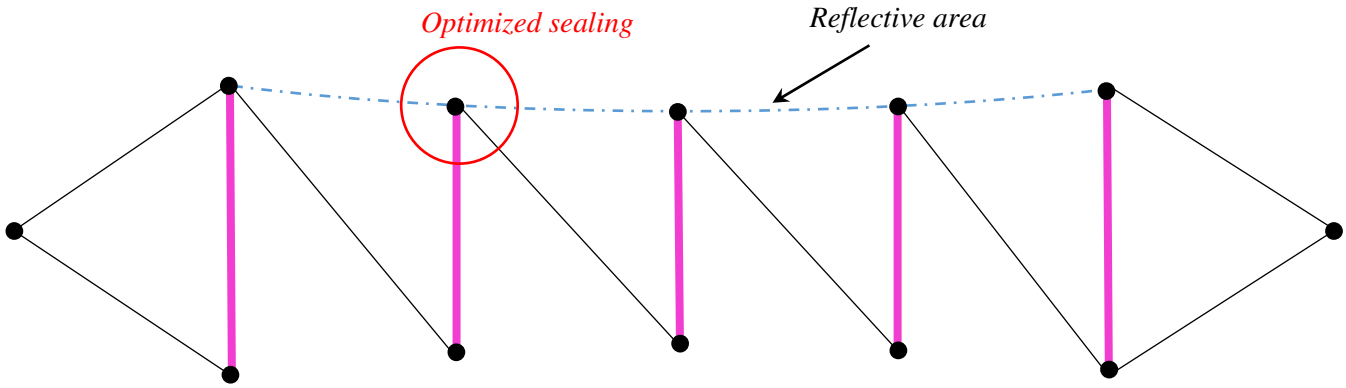

Fig. 12. Unencumbered the reflective surface of a pyramidal network

Moreover, Fuller and Geiger type cable dome structures require that the upper and lower part of the reflector have the same (orientation) convexity in order to have the bars compressed, this is not the case with a the pyramidal network.

Figure 14 shows the distribution of bars for the different types of networks. Compared to the other cable domes, the pyramidal network allows for have control points distributed on a triangular equilateral mesh, regardless of the bars, with the distance between any two consecutive bars being identical. This pattern of bar distribution allows for a more optimal distribution of forces in the network.

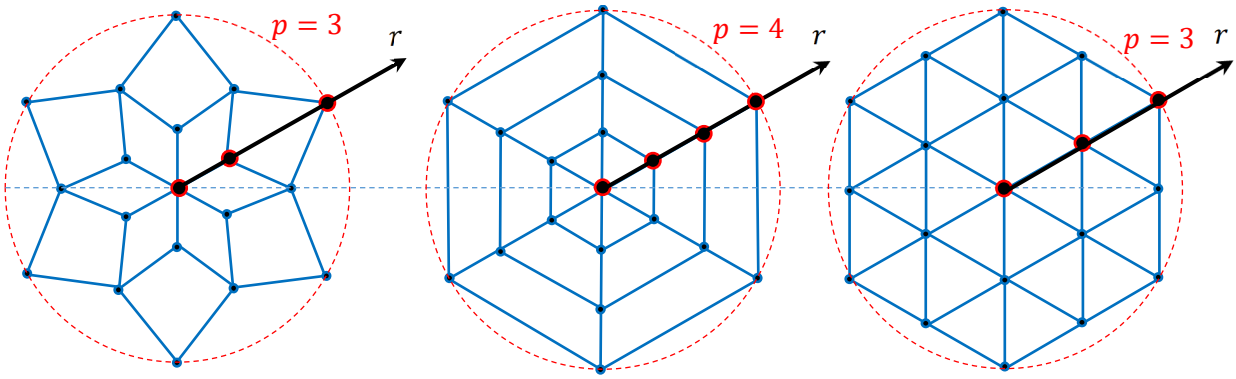

Fig. 14. Distribution of bars for various configurations (19 bars).

Defining p the maximum number of bars on the radius r, the number of hook points for membrane in function of p for the different networks, is listed below in Tab. 1.

Fuller	Geiger	Pyramidal
$6p + 1$	$6(p - 1) + 1$	$3(p - 1)p + 1$

Tab. 1. Number of bars for a given radius

As can be seen, the number of bars that can be inserted is of the order of $3p^2$ for a pyramidal network compared to the Fuller and Geiger networks which are both of the order of $6p$. This density of points in the mesh makes it possible to cover a larger area of membrane peaks and troughs, and avoids the need to privilege a radial distribution on which points need to be located.

Figure 15 shows the spatial configuration of pyramidal networks for $p = 2$ and $p = 3$.

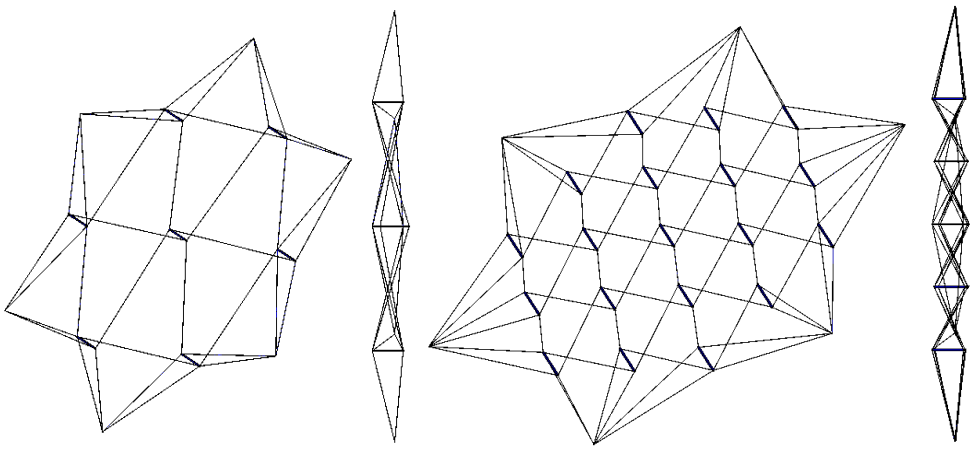

Fig. 15. Pyramidal networks for $p = 2$ and $p = 3$ (configuration (2))

In order to determine the axial forces across the network in an analytical manner in section II, it is necessary to determine the different geometric variables involved in the design of the network.

This section will focus on a 19-bar configuration pyramidal network $(p = 3)$ as presented (Fig. 16.). T is the tension introduced by the flexional energy stored in the joints of the peripheral ring.

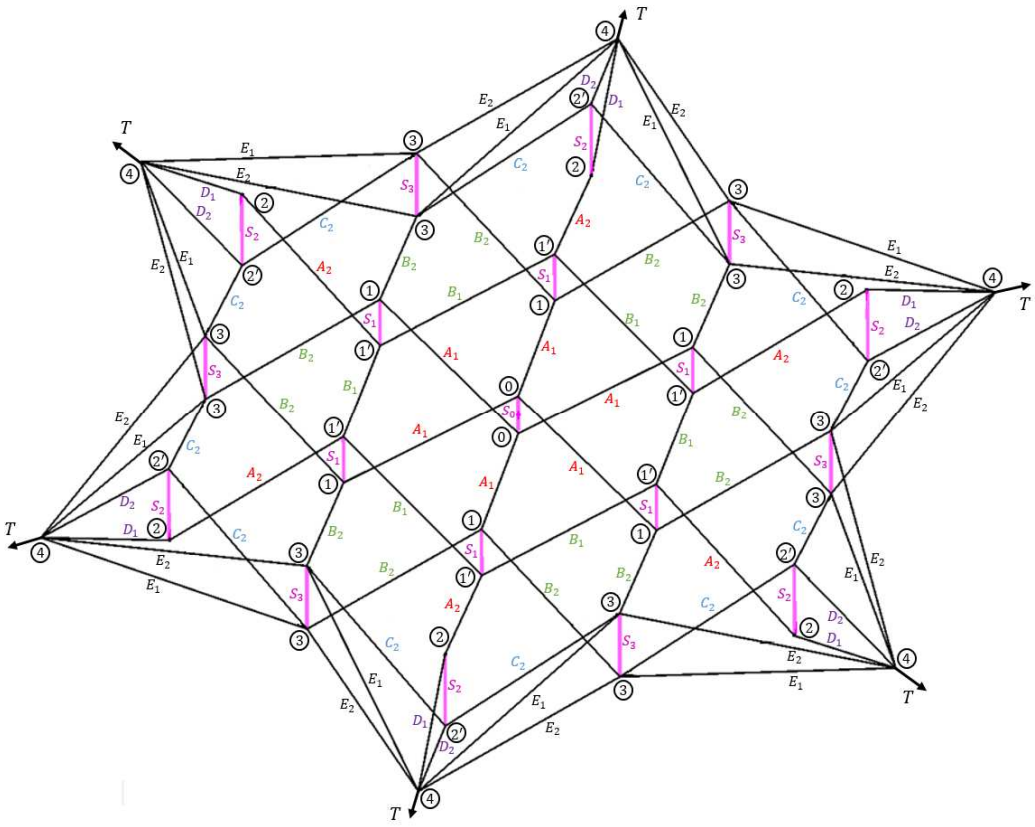

Fig. 16. Geometric variables of the pyramid network

A comparison with the numerical model was then made in order to validate the analytical model. The network is configured using the bar height at the center h_0, ΔX being the distance between any two consecutive bars, the focal length F and where d_0 is the distance between the bar S_2 and the anchorage point (4). The various resulting geometric variables are shown in Figures 17 to 20.

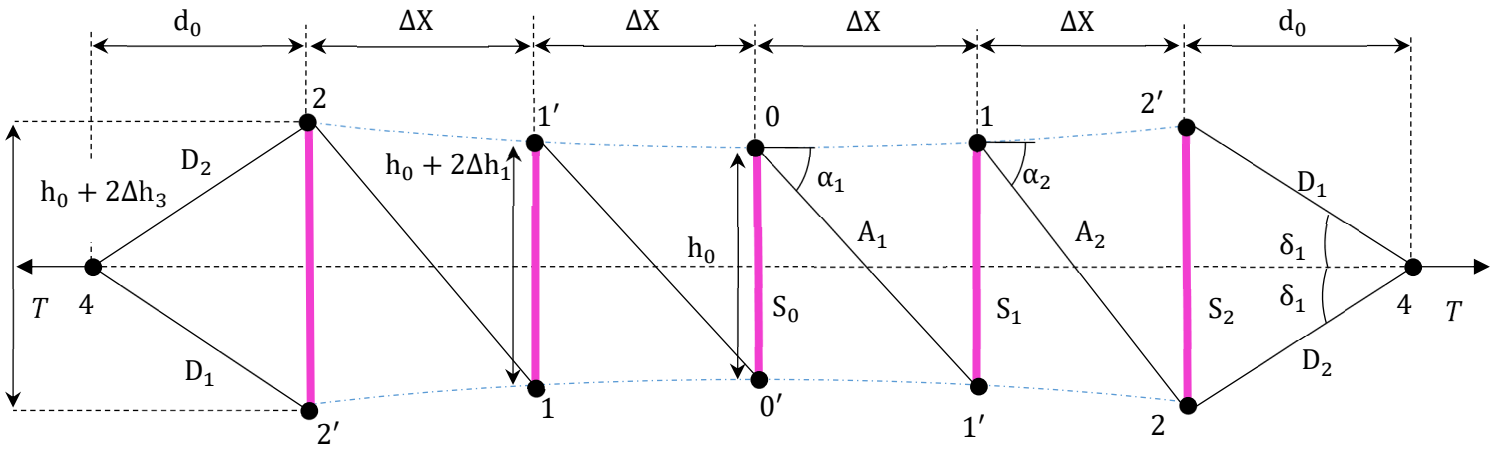

Fig. 17. View of the network in the plane comprising nodes 0, 1, 2, 4.

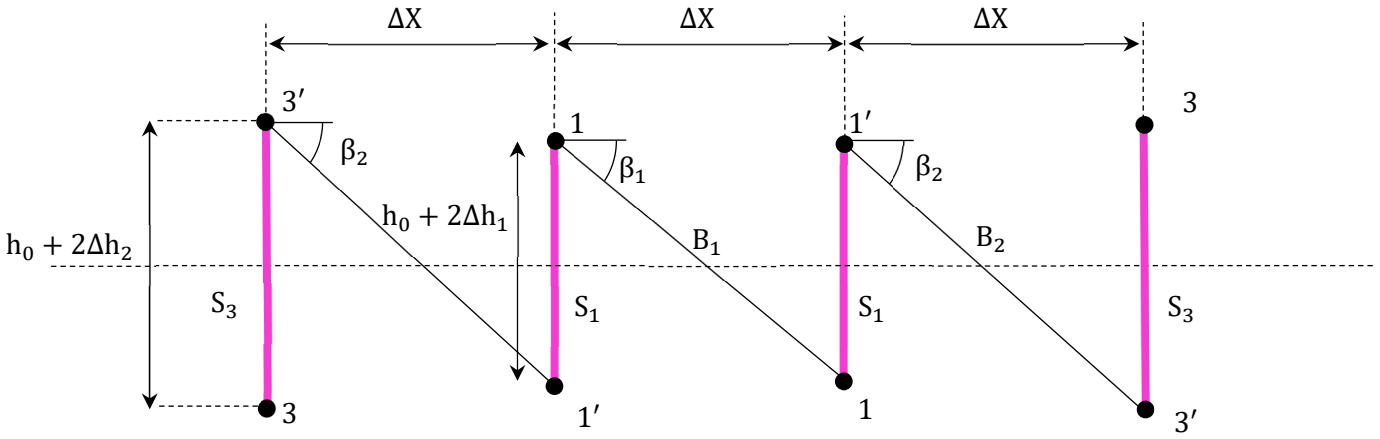

Fig. 18. View of the network in the plane containing the nodes 1, 1', 3, 3'

The geometric parameters of the systems peripheral rigging are shown in Figure 19.

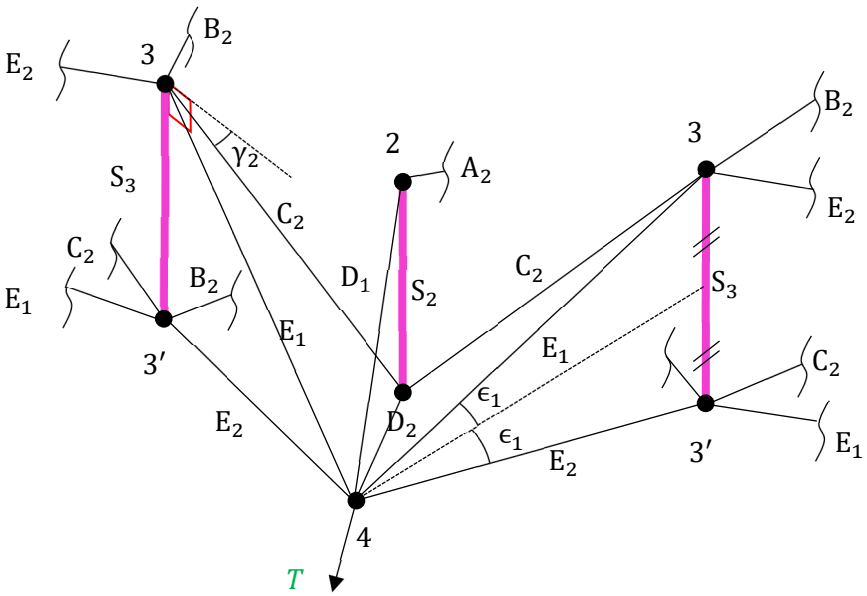

Fig. 19. The peripheral geometric parameters of a standard network.

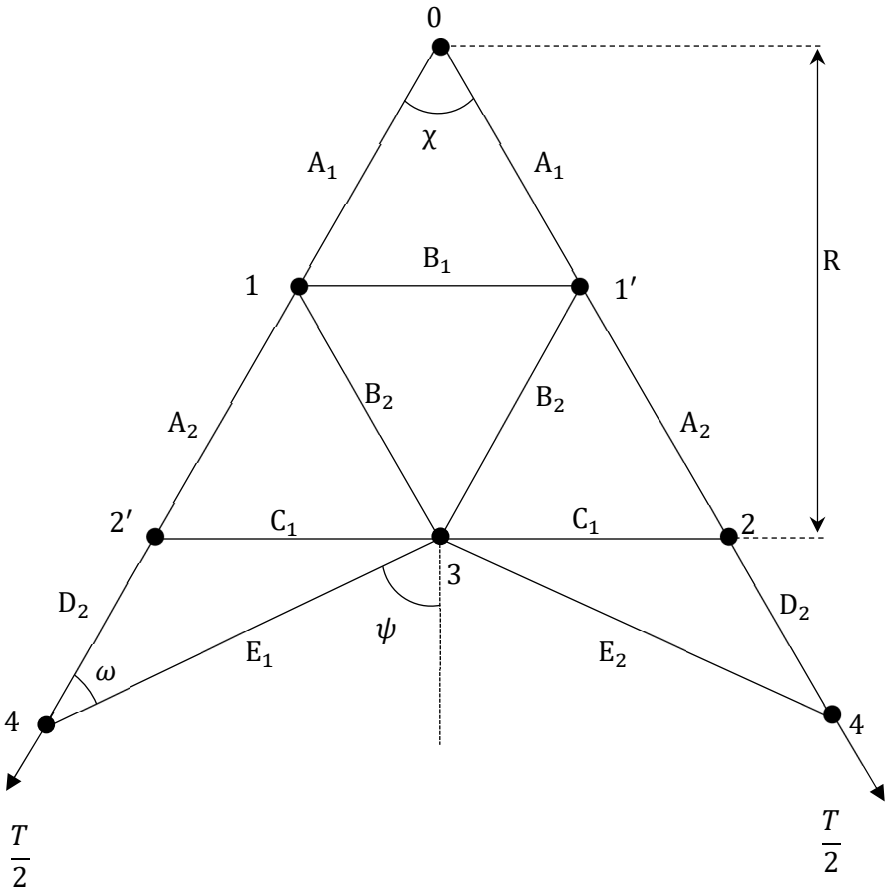

Fig. 20. Top view of a portion of a pyramidal network

For a space antenna, as a function of their mission, the geometrical input parameters are the focal length F, and the radius of the reflective area R. For a fixed geometry (F, R), it's possible to optimize the network as a function of p, h_0 and d_0 acting directly on the angular parameters and consequently on Δh_i. The geometry of the system depends on the focal length of the parabola marked F, the height of the bars, whose reference height h_0 is that of the central bar. ΔX is the distance between any two consecutive bars of the network. The angles α_i, β_i, γ_i are respectively the complementary angles formed by the cables A_i, B_i ,C_i with the bar and projection. The distance between the application point of the force T and the S_2 bar is defined by d_0. In this configuration, $\chi = \frac{\pi}{3}$, and the fixed parameters are $h_0, d_0, \Delta X$, F and p. The various relational parameter necessary to solve the equations are given in Table 2.

Angular parameters	**Length parameters**
$\alpha_1 = \operatorname{atan}\frac{h_0 + \frac{\Delta X^2}{4F}}{\Delta X}$	$\Delta h_1 = \frac{\Delta X^2}{4F}$
$\alpha_2 = \operatorname{atan}\frac{h_0 + \Delta h_1 + \Delta h_3}{\Delta X}$	$\Delta h_2 = \frac{3\Delta X^2}{4F}$
$\beta_1 = \operatorname{atan}\frac{h_0 + 2\Delta h_1}{\Delta X}$	$\Delta h_3 = \frac{\Delta X^2}{F}$
$\beta_2 = \operatorname{atan}\frac{h_0 + \Delta h_1 + \Delta h_2}{\Delta X}$	
$\gamma_2 = \operatorname{atan}\frac{h_0 + \Delta h_2 + \Delta h_3}{\Delta X}$	
$\delta_1 = \operatorname{atan}\frac{h_0 + 2\Delta h_3}{2d_0}$	
$\epsilon_1 = \operatorname{atan}\frac{h_0 + 2\Delta h_2}{2\sqrt{\left(\frac{\Delta X}{2} + d_0\right)^2 + \left(\Delta X \cos\frac{\chi}{2}\right)^2}}$	
$\psi = \operatorname{acos}\frac{d_0 \cos\frac{\pi}{6}}{\sqrt{\left(\frac{\Delta X}{2} + d_0\right)^2 + \left(\Delta X \cos\frac{\chi}{2}\right)^2}}$	
$\omega = \psi - \frac{\chi}{2}$	

Tab. 2. Geometrical parameters of the modelling

II.2 Axial forces distribution

II.2.1 Static calculus: analytical model

The current standard system, comprising of 19 bars and 66 cables. There are 13 independent equations for 13 unknowns written in APPENDIX A giving the forces according to the geometry and the tension introduced into the network by the peripheral ring.

In order to solve the system, the axial forces are written based on the normal force of the central bar noted S_0. For this, the equations are written step by step starting from the central node 0 to the node 4 attached to the ring.

II.2.2 FEM model and comparison between analytical and numerical model

To assess the consistency of the analytical model, a finite element model was developed under Ansys®. The model is composed of bar elements (3 DOF per node). The modelling assumes that the nodes on which the cables at node 4 are anchored and a force is exerted on the central bar (Fig.21.).

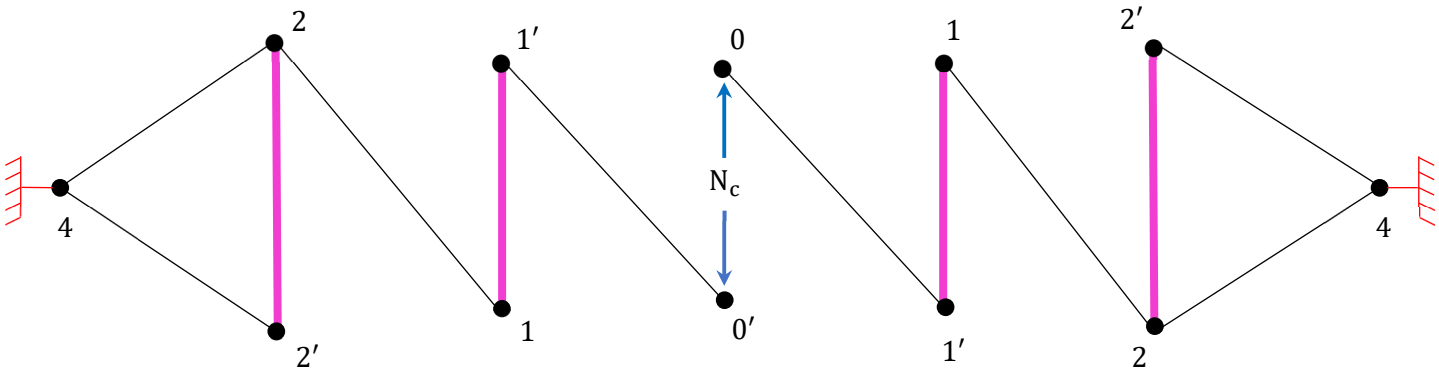

Fig. 21. Geometric parameters of standard network stowage.

The network bars forming the hooking points are composed of carbon epoxy circular solid section with a modulus of elasticity of 125GPa with a 78,5mm² cross section. The cables connecting the bars are made of kevlar (elastic modulus E=125GPa, section 20mm²). The network's geometric parameters for $h_0 = 0.2$m are given in Table 3. The focal length of both sides of the network (illuminated and rear) is set at to $F = 4.5$m for all simulations. The diameter of the reflective surface is $\phi = 2R = 2.2m$.

Angular parameters	rad	(°)	Length parameters	(m)
α_1	0.34	19.32	F	4.50
α_2	0.46	26.18	ΔX	0.634
β_1	0.37	21.10	h_0	0.200
β_2	0.43	24.53	Δh_1	0.022
γ_2	0.51	29.34	Δh_2	0.067
δ_1	0.39	22.20	Δh_3	0.089
ϵ_1	0.17	9.92	d_0	0.464
ω	0.61	35.11	ϕ	2.20
ψ	1.14	65.11		

Tab. 3. Geometric parameters of the standard network for $h_0 = 0.2\ m$.

Simulations were performed for h_0 bar heights of 0.2m, 0.4m and 0.6m, with T tension ranging from 50N to 300N. Results are shown in Table 4.

	$h_0 = 0.4\ m$								
	50 N		**100 N**		**200 N**		**300N**		
Cables	**Ana.**	**FEM**	**Ana.**	**FEM**	**Ana.**	**FEM**	**Ana.**	**FEM**	**e**
A1	12.11	12.11	24.28	24.28	48.37	48.38	72.59	72.60	0.01%
A2	12.95	12.94	25.96	25.95	51.73	51.71	77.63	77.60	0.04%
B1	12.31	12.30	24.68	24.67	49.17	49.15	73.79	73.75	0.05%
B2	12.73	12.72	25.52	25.51	50.86	50.82	76.32	76.26	0.07%
C2	8.06	8.06	16.17	16.16	32.21	32.19	48.34	48.31	0.07%
D1	11.88	11.87	23.81	23.80	47.44	47.42	71.20	71.16	0.05%
D2	7.14	7.14	14.32	14.31	28.54	28.52	42.82	42.80	0.05%
E1	10.18	10.17	20.41	20.39	40.67	40.63	61.03	60.97	0.09%
E2	11.35	11.34	22.76	22.74	45.34	45.30	68.04	67.98	0.09%
Bars	**Ana.**	**FEM**	**Ana.**	**FEM**	**Ana.**	**FEM**	**Ana.**	**FEM**	**e**
S0	-20.14	-20.15	-40.38	-40.40	-80.45	-80.50	-120.73	-120.80	0.06%
S1	-22.27	-22.26	-44.65	-44.64	-88.96	-88.94	-133.50	-133.46	0.03%
S2	-14.42	-14.41	-28.90	-28.89	-57.59	-57.56	-86.43	-86.37	0.06%
S3	-18.89	-18.88	-37.88	-37.86	-75.49	-75.43	-113.28	-113.19	0.08%

Tab. 4. Normal forces in the elements in function of T for $h_0 = 0.4m$.

e $=$ the maximum relative deviation of the data series from FEM and the analytical model.

The results showed that whatever the load case, the relative deviation was less than 0.4% for the majority of simulations and less than 2.53% when $h_0 = 0.05\text{m}$. These results validate our analytical model. As can be seen in Figure 22, for the same configuration, the normal stress in the elements varies linearly depending on the input tension T. Regardless of the bar height h_0, the graphs have the same profile.

Moreover, the difference of the tensions in the central cables is very small, the principal differences being noted for the peripherals cables. Compared to Fuller and Geiger networks that only recover 18% of T tension from Fayos [13], this network can achieve more than 25% at the center.

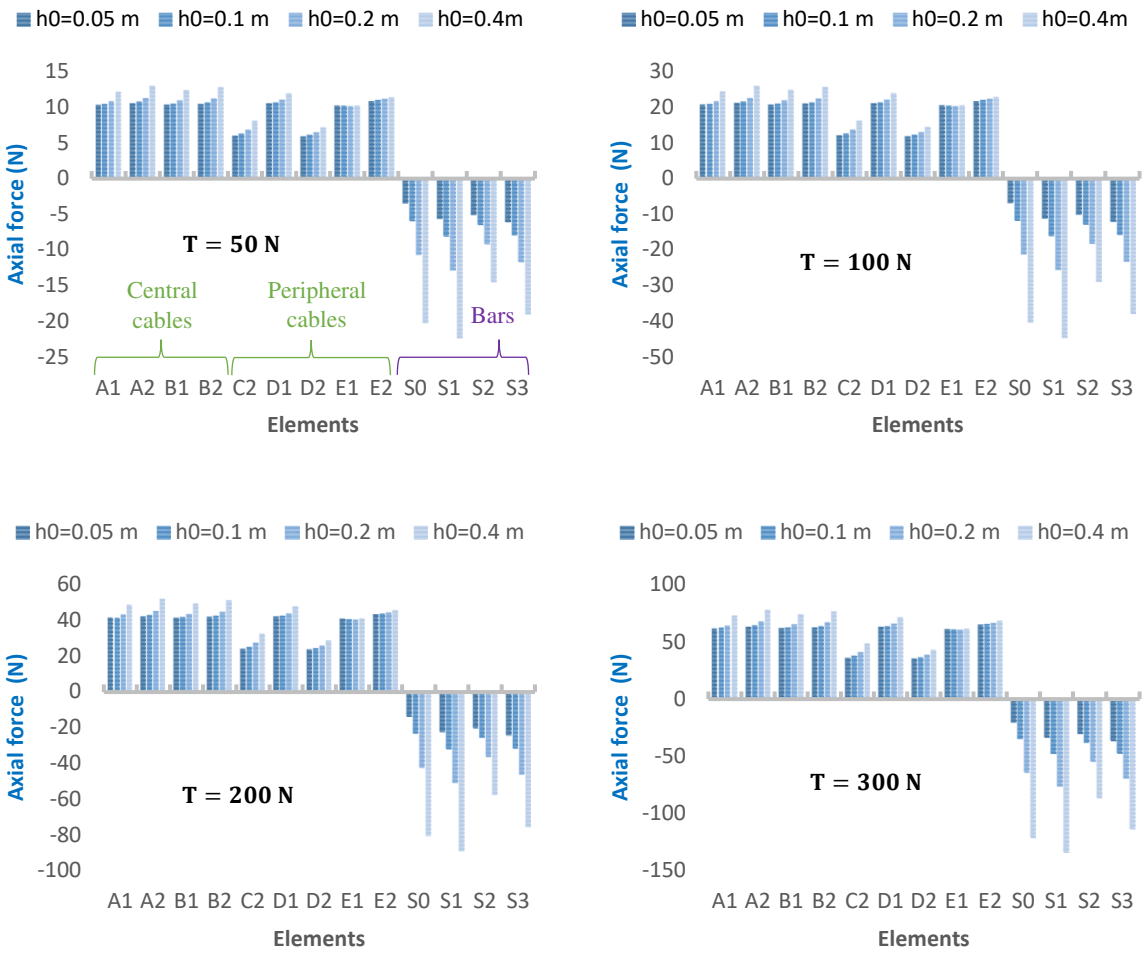

Fig. 22. Axial forces in elements depending on height h_0 for various input tensions

III Network optimization and space antennas applications

In order to ensure optimal tension efficiency, it is important to consider the position of the network (configuration 1 or 2) in relation to the antenna skeleton, as well as the different parameters that influence the operational phase. A membrane is added to this network to complete the system and modal analyses are performed.

III.1 Optimizing network configuration

III.1.1 Network anchoring configurations

The results of the simulation presented in Table 5 show that for the same geometry, the mechanical performance at the usable area of the configuration (2) was less efficient than the configuration (1). For a given peripheral ring geometry, configuration (2) allows a better network arrangement than configuration (1), but the latter is not mechanically optimal due to the high angle values formed by the peripheral cables (Fig.23).

	Configuration 1		**Configuration 2**	
	Axial force (N)	**Ratio N_i/T**	**Axial force (N)**	**Ratio N_i/T**
T	**100**		**100**	
A1	21.627	21.6%	19.376	19.4%
A2	22.571	22.6%	16.744	16.7%
B1	21.680	21.7%	18.419	18.4%
B2	22.162	22.2%	20.299	20.3%
Standard deviation	**0.445**		**1.517**	
S0	-22.022	22.0%	-23.524	23.5%
S1	-25.716	25.7%	-23.160	23.2%
S2	-18.030	18.0%	-18.647	18.6%
S3	-23.002	23.0%	-17.081	17.1%
Standard deviation	**3.185**		**3.230**	

Tab. 5. Distribution of the tensions in the elements under FEM for $h_0 = 0.2m$.

N_i designate the normal force in an element i (bar or cable) of the cable net.

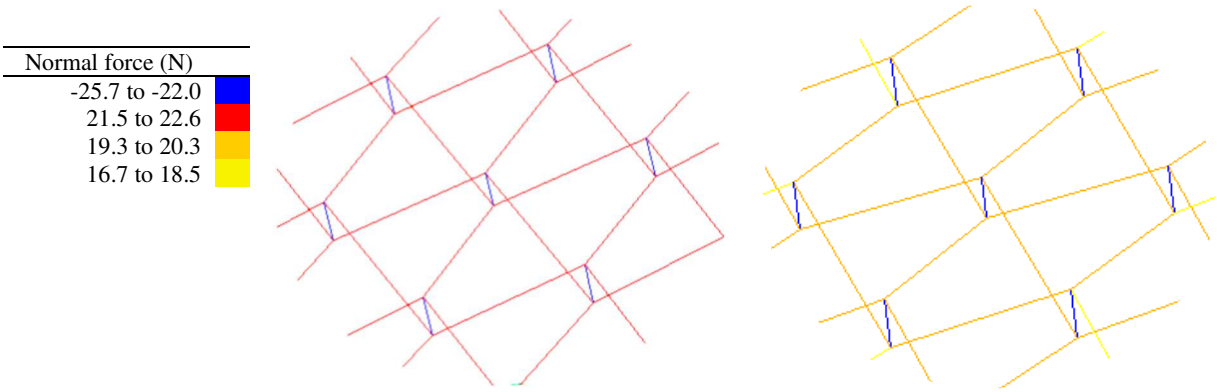

Configuration (1) Configuration (2)

Fig. 23. Tension distribution in various elements for both configurations.

III.1.2 Distribution of the axial force for configuration (1)

By tending the focal point towards the infinity, you get a flat grid. Table 6 represents the distribution of the forces for a tension of 200N. The relative discrepancy between the two configurations of Table 6 is fairly small, showing a quasi-uniform tension in the parabolic network.

	Focal (m)	∞	**4.54**	
		Normal force (N)	**Normal force (N)**	**Relative deviation**
Cables	A1	42.00	42.78	1.87%
	A2	42.00	44.96	7.06%
	B1	42.00	43.27	3.02%
	B2	42.00	44.36	5.62%
	C2	26.34	27.18	3.16%
	D1	40.97	43.58	6.37%
	D2	25.70	25.60	0.40%
	E1	38.60	40.19	4.11%
	E2	44.25	44.13	0.27%
Bars	S0	-37.90	-42.44	11.96%
	S1	-37.90	-50.89	34.27%
	S2	-21.27	-36.19	70.17%
	S3	-29.19	-46.13	58.02%

Tab. 6. Tension distribution in the various elements for two different focal lengths $h_0 = 0.2m$ and T=200N

Tensions in the central elements for the infinite focal length network (Fig. 24) are homogenous. Indeed, the following relationships for an infinite focal length are obtained:

$$A_1 = A_2 = B_1 = B_2 \tag{15}$$

$$S_0 = S_1 \tag{16}$$

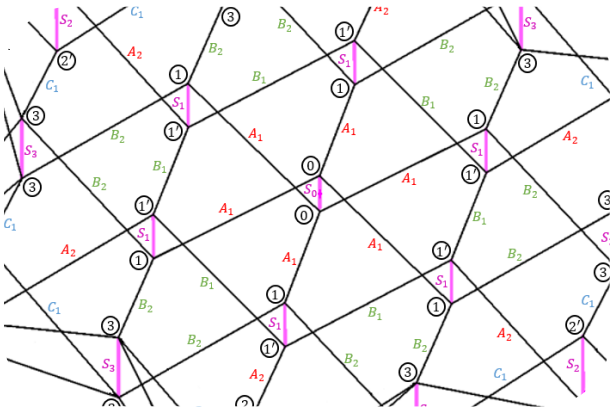

Fig. 24. View of the central network

However, not all stresses in the bars and cables of the internal part of the network are homogeneous. The tension is not uniform in the certain elements due to edge effects. The reflectors need to have very high accuracy in the centre of the reflector surface. By increasing the number of bars within the network, it can be seen numerically that the tension is uniform in the elements located toward the centre. A study of network densification showed that the distribution of axial forces at the center was almost uniform for a 61-bar structure (Fig. 25).

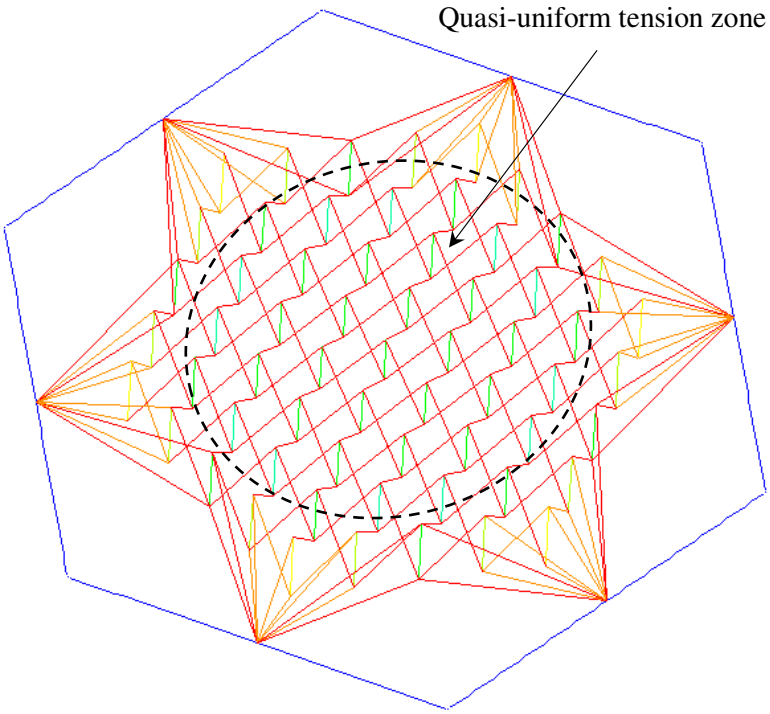

Fig. 25. Distribution of axial force in the network for $p = 5$

III.2 Configuration (1) Network attachment

The vibratory environment of the satellite is a major constraining element for space structures. Studies carried out [6] showed that the frame was perfectly in line with the specifications, that is to say, greater than 1Hz to prevent interaction with the Attitude Control System of the Satellite. Due to side effects, the standard pyramidal network contains solid mechanisms at the periphery (Fig. 26). When considering the network as a single entity, some bars are not laterally stabilized. Infinitesimal mechanisms are also present between crowns of bars and stabilisation can be achieved by the addition of bracing cables avoiding rotation of the crowns one to other.

In order to take into account the influence of the bracing elements of the structure, a static analysis was carried out. The influence of the presence of the cables as well as their tensioning is presented in part **IV.2**.

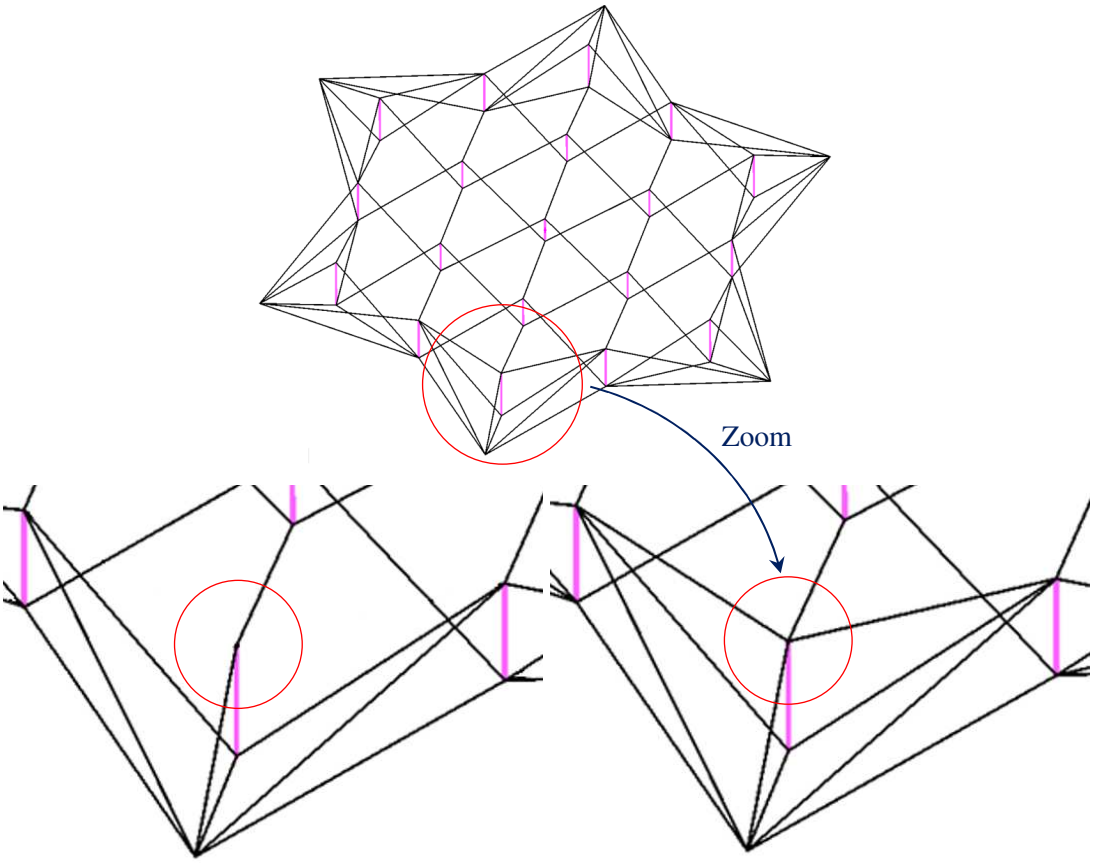

Configuration (1.a) **Configuration (1.b)**

Fig. 26. Network attachment mechanism a) and braced system b)

To avoid mechanisms, bracing cables were inserted (Fig .27).

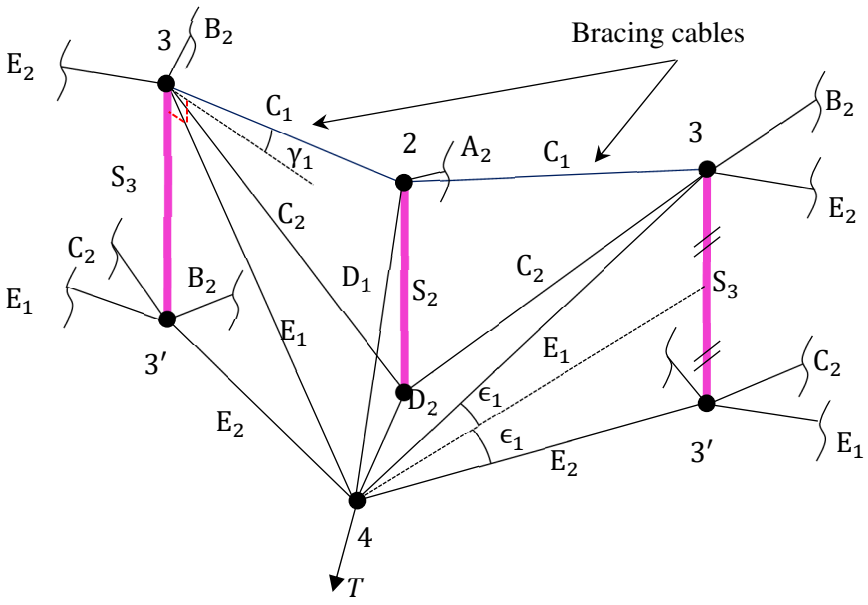

Fig. 27. Geometric docking parameters for the reinforced network.

III.3 Study of a definitive solution

III.3.1 Reflective shape

III.3.1.1 Static analyses of the antenna with the standard network

To evaluate the influence of the membrane on the antenna, numerical simulations were performed with the configuration (1.a) (without bracing cable). The membrane was made of SHELL181 elements under Ansys®, isotropic material with a Young modulus $E_m = 15.10^9$Pa, and a thickness of 0.1mm. Results of the simulations are shown in Table 7.

	Element	Network Ansys (N)	Network Analytical (N)	Relative difference	Network with Membrane	Relative difference
	Tension T	100	100			
Inner cables	A1	21.23	21.39	0.7%	21.13	0.5%
	A2	22.34	22.48	0.6%	19.49	12.8%
	B1	21.51	21.63	0.6%	18.76	12.8%
	B2	22.01	22.18	0.8%	18.37	16.6%
Peripheral cables	C1	-	-	-	-	
	C2	13.48	13.59	0.8%	11.82	12.3%
	D1	21.65	21.79	0.6%	19.29	10.9%
	D2	12.71	12.80	0.7%	11.14	12.3%
	E1	19.91	20.09	0.9%	18.62	6.5%
Bars	S0	-21.21	-21.22	0.0%	-21.22	0.0%
	S1	-25.33	-25.45	0.5%	-25.21	0.5%
	S2	-17.96	-18.09	0.7%	-15.83	11.9%
	S3	-22.90	-23.06	0.7%	-21.21	7.4%

Tab. 7. Tension distribution in the various elements for a naked network and network with membrane solution $h_0 = 0.2m$.

Bars elements are compressed and cable elements are tightened, the system is properly designed.

III.3.2 Static analyses of the antenna with the reinforced network

To tension the reinforced cable-dome (configuration 1.b) in the FEM, the tension T is directly introduced at point 4, locking all rotation and displacement along the z axis. In order to validate the FEM modeling, equations are solved analytically. To evaluate the normal force in the bracing cable C_1, the Castigliano theorem was applied (1):

$$\sum_{i=1}^{n} \frac{1}{E_i S_i} \int_0^{\ell_i} N_i(X) \frac{\partial N_i(X)}{\partial X} dX = 0 \qquad (1)$$

With N_i and E_i are, respectively, the normal force in the element i, the Young modulus of the bar i, ℓ_i is the length of the element i and S_i the section of the element i. Numerical and analytical results with $T = 50N$ and $h_0 = 0.2m$ are shown for each bar in Table 8.

	Elements	Analytical Method	FEM	Error
Inner cables	A1	9.56	9.70	1.4%
	A2	10.04	10.18	1.3%
	B1	9.67	9.81	1.5%
	B2	9.91	10.06	1.5%
Peripheral cables	C1	3.43	3.38	1.5%
	C2	6.94	7.41	6.4%
	D1	13.43	13.67	1.8%
	D2	6.53	6.99	6.5%
	E1	6.64	6.54	1.5%
	E2	12.20	12.60	3.2%
Bars	S0	-9.48	-9.61	1.3%
	S1	-11.37	-11.52	1.3%
	S2	-9.24	-9.85	6.2%
	S3	-10.61	-10.93	2.9%

Tab. 8. Tensions of the reinforced network calculated analytically and numerically

Using analytical models of the standard (configuration 1.a) and reinforced (configuration 1.b) cable dome, coefficients of correlation have been calculated for the inner cables of the cable dome. Whatever the tension T and h_0, the coefficient of correlation for the tension in the cables in the inner part is equal to 1, indicating the linearity between standard and reinforced networks. The results of the ratio $\frac{T_{iso}}{T_{hyper}}$ are presented for a tension $T = 100N$ as a function of h_0 in Figure 28.

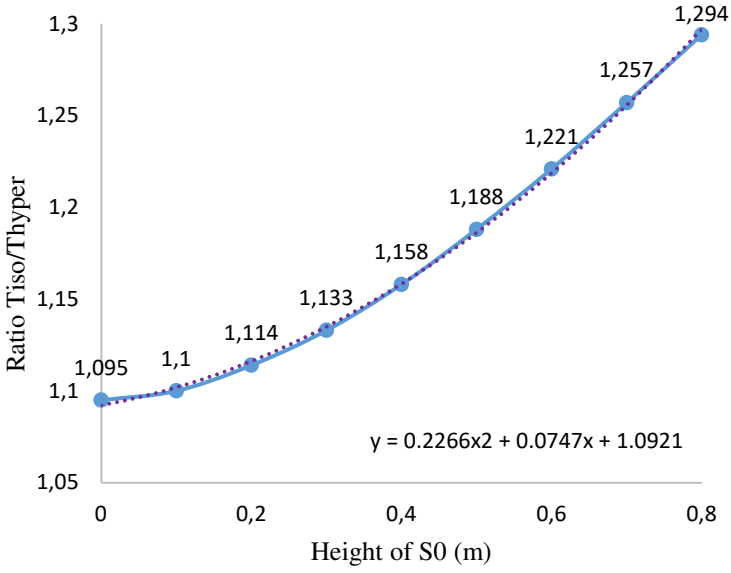

Fig.28. Coefficient as a function of the height for the inner cable.

To obtain the optimal geometrical configuration that gave a suitable tension in the network, lengths of cable dome bars are changed and the results are given as a function of the maximum absolute value in the cable and in the bar. So, ratios A_2/T and S_2/T are given as a function of h_0 (Fig.29). Results showed that the absolute value of the normal force in the bar rise as a function of the length of the bar.

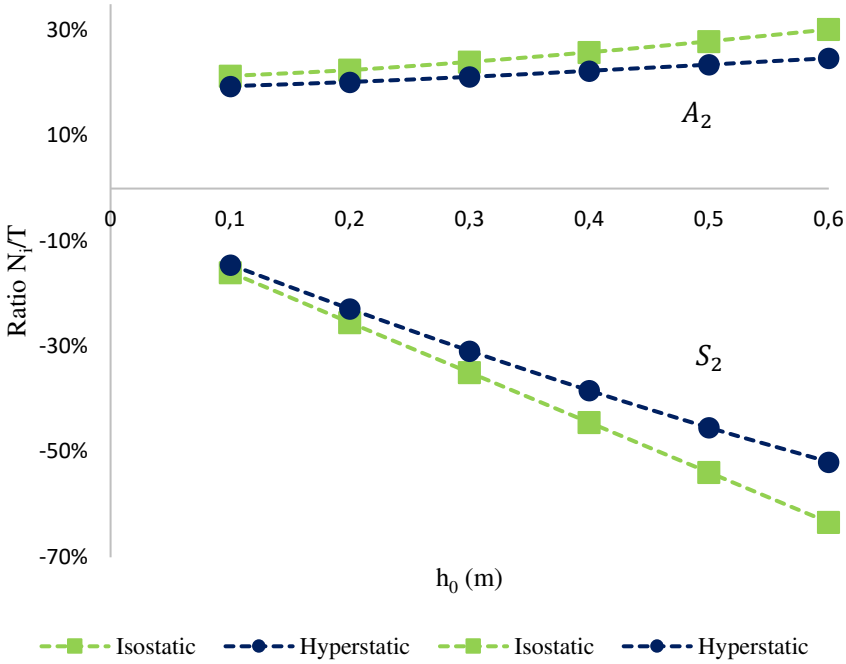

Fig.29. Ratio N_i/T in function of h_0.

In order to study a complete solution, the peripheral hexagonal ring is added at the membrane system. The maximum value of the Von Mises stress is located at the attachment point of the shape. For these simulations, $h_0 = 20cm$, $E_m = 10GPa$ and cable dome bars were 1cm diameter (Fig.30). Results show that the model is quasi linear.

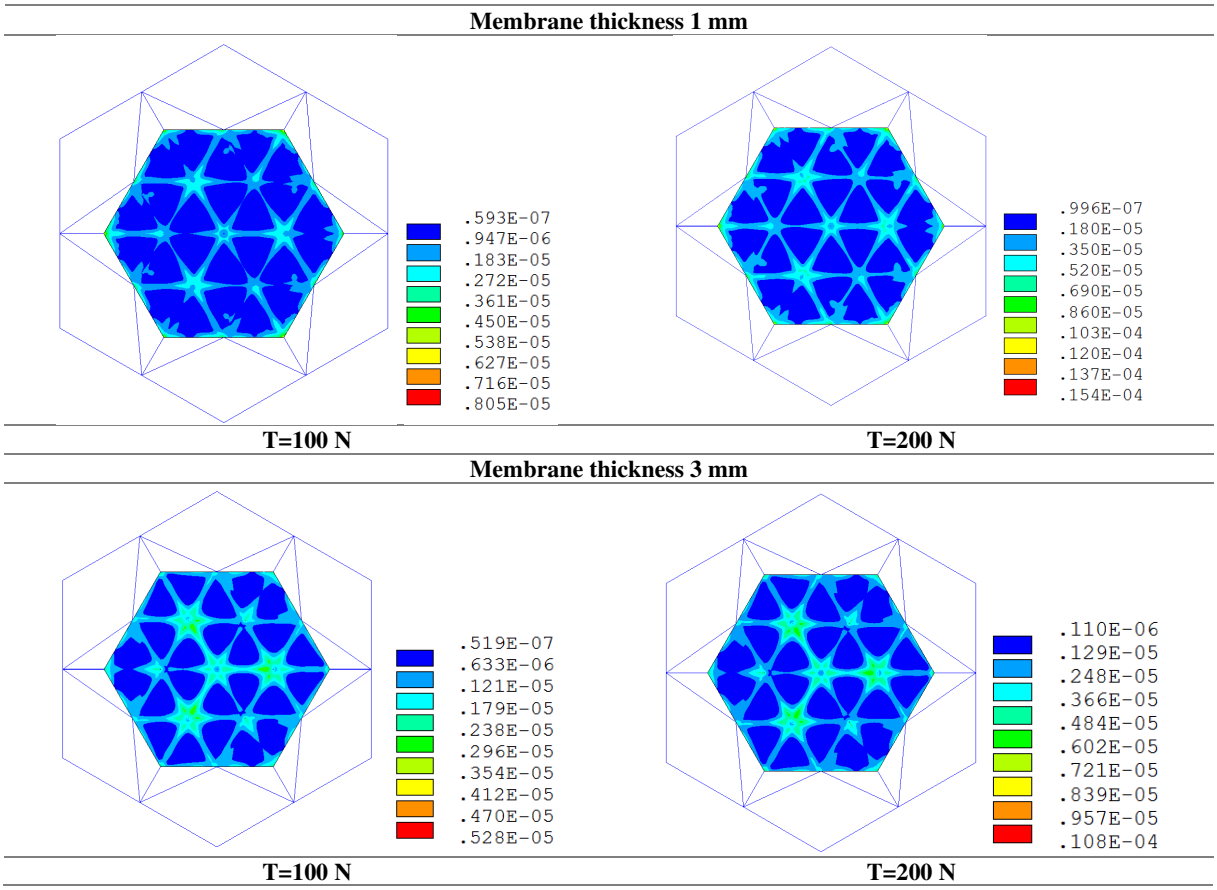

Fig. 30. Distribution of stresses on the membrane

The cable net possessed a third order circular symmetry. Stresses on the shape are distributed along the edge of triangular pattern and are maximals at the anchor points of the membrane with the bars of the cable dome (Fig.30).

III.3.1.3 Modal analysis of the concept

In order to evaluate the potential of this antenna in an operational configuration, a modal analysis was performed numerically. Generally, the first eigenfrequency of a space deployable antenna is low. Tzerodz [17] presents a circumferential ring architecture of a conical V folded shape and 4m diameter with a first frequency of 0.472Hz. Similary, Medzmariashvili [18] presents a conical frame with a diameter of 6m with a first mode of 0.624Hz, with an antenna is around 13kg. In our case, the requirement of the first eigenfrequency of the antenna must be higher than 1Hz. A bar of the peripheral rim of the antenna is embedded in the middle. The geometrical and mechanical parameters of the simulation are presented in Table 9.

	Mass (kg)	Number of elements	Element type
Cable dome bars	vary	19	LINK180
Peripherals wires	0.808	42	LINK180
Cable dome wires	1.014	48	LINK180
Rim bars	2.863	192	BEAM188
Membrane	0.315	9600	SHELL181

Tab. 9. Parameters of the simulation

A modal analysis, using bending prestressing uses the linear perturbation method as defined in Ansys®, was carried out. The ring was prestressed by reducing the length of the cables, generating a compressive moment and force in the ring. The deformation coefficient of the element was calculated using numerical simulations and calibrated using equation (A.13), defined in Annexe A, by imposing the tension T.

The ring is composed of carbon tubes of circular hollow cross section, elastic modulus $\mathrm{E_t} = 125\mathrm{GPa}$, density $\rho_t = 1550\ \mathrm{kg/m^3}$, thickness $\mathrm{e_t} = 1\mathrm{mm}$, diameter 5cm, shear modulus $\mathrm{G_t} = 90\mathrm{GPa}$. The results are presented in the following table for the structure with a total ring mass of 2.86kg and with a 2m bar length. The standard network was considered. Results for a simulation with $T = 100\mathrm{N}$, $h_0 = 0.2\mathrm{m}$, a membrane thickness equal to 0.3mm and various density ρ_m and Young modulus E_m of the membrane are presented in Table 10.

ρ_m ($\mathrm{kg/m^3}$)	750	850	950	1050
	F1 (Hz)	**F1 (Hz)**	**F1 (Hz)**	**F1 (Hz)**
$E_m = 1\mathrm{GPa}$	2.4356	2.3993	2.3609	2.2890
$E_m = 10\mathrm{GPa}$	2.5232	2.5082	2.4789	2.4574
Antenna mass (kg)	6.1494	6.2701	6.3909	6.5117

Tab.10. First eigen frequencies in function of the density and Young modulus

Results show that for various configurations, the first frequency is higher than 1Hz.

As seen (Fig.31), the first mode is a flexional mode, corresponding to the first mode of the ring, as described by Bettini [6].

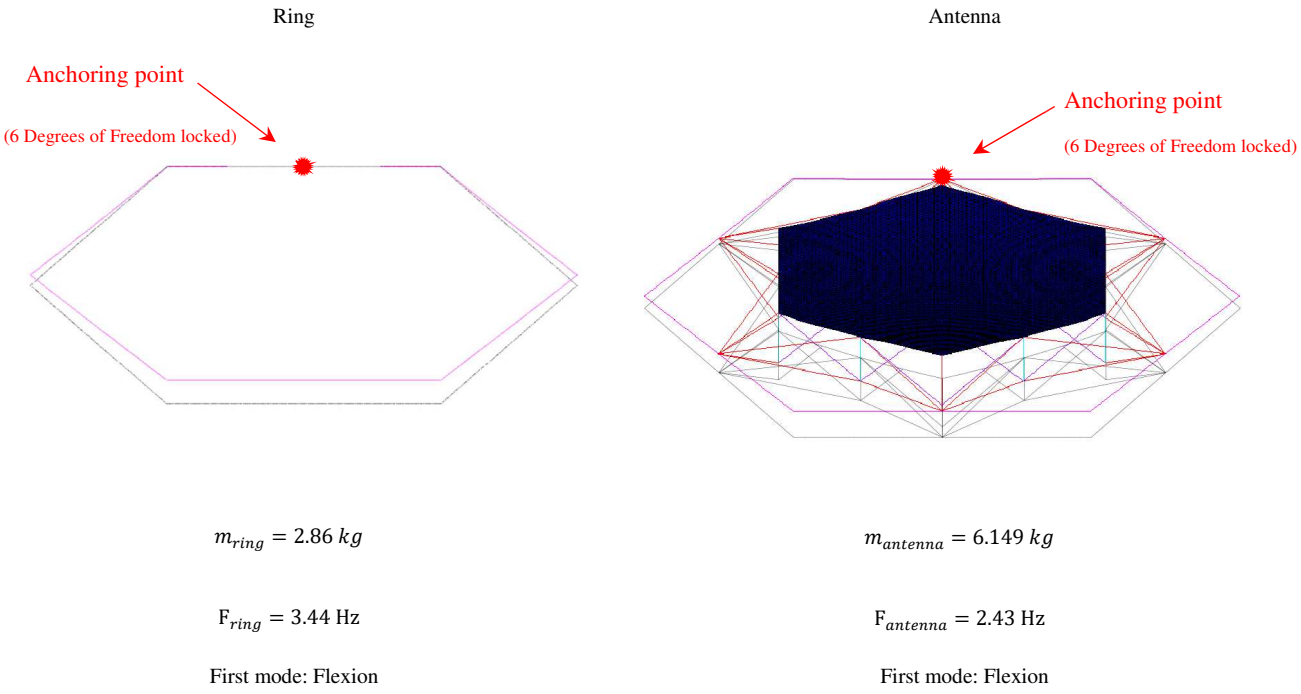

Fig. 31. Shape of the first mode of the ring and of the antenna (standard)

By increasing the length of the bars, it would also be possible to extend the concept to larger diameters antennas. It can be observed that by comparing the ratio of the natural frequency of the ring to that of the square root of the antenna mass to the ring mass, the results are very close Eq. 2.

$$\frac{f_{antenna}}{f_{rim}} = \frac{2.43}{3.44} = 0.706 \; and \; \sqrt{\frac{m_{ring}}{m_{antenna}}} = \sqrt{\frac{2.863}{6.149}} = 0.682 \qquad (2)$$

Thus the frequency of the first mode would not depend on the size of the reflecting surface but highly on its mass.

$$f_{antenna} \approx f_{rim} \sqrt{\frac{m_{ring}}{m_{antenna}}} \qquad (3)$$

Hence, by optimising the ratio $\frac{m_{ring}}{m_{antenna}}$ and the mass of the ring thanks the use of lightweight and high-performance materials such as CFRP materials (allowing to reduce the thickness of bars down to 0.1mm) for the ring and the dome cable bars, the natural frequency of the antenna can be optimised.

For example, considering a ring composed of bars of length 3m, a useful surface of about 6m could be achieved. Using Eq. 3, with $\frac{\mathrm{m_{ring}}}{\mathrm{m_{antenna}}} \approx 0.5$ and a $\mathrm{f_{rim}} = 1.92\mathrm{Hz}$ (made of carbon epoxy, with bars diameter =7.5cm, bars thickness =1mm), $\mathrm{f_{antenna}} \approx 1.35\mathrm{Hz}$.

IV. Summary and conclusion

This paper presents a new concept of a three-dimensional network and space antenna. It is attractive because of its simplicity, and the homogeneous distribution of control points allowing a more optimal distribution of axial forces within the network. Another advantage of this solution is the requirement for a simpler ring structure. In comparison with conventional cable domes of the Fuller and Geiger type, the transmission of forces is more homogeneous. Another advantage of this network is that it is not necessary to have two convex surfaces in order to obtain a three-dimensional network. Various models were presented: an analytical standard network model and a numerical model. The gap between the standard analytical model and the numerical model is very small < 0.4%. This difference is further reduced by a larger height of the $\mathrm{h_0}$ bar. As a result, the use of the analytical model allows a very rapid sizing of the network by the designer. An optimal network configuration can be calculated based on various geometric parameters: focal length, network bar height, allowing rapid sizing. The uniform tension allows us to approach at best a parabolic surface.

A first study verified that the antenna satisfied the frequency criteria. The influence of different parameters on the first mode such as the tension T, the height of the bars of the network, the mass of the nodes of the ring, the network type (standard or reinforced) and the thickness of the membrane must be evaluated.

A more detailed study on the adaptation to large diameters should be carried out.

Exposure to sunlight will affect both the behavior and the RMS (surface accuracy) error of the network and the tensioned membrane. Thermal aspects of the environment will need to be considered in the modelling in order to assess the behavior of the rim, of the membrane and the dome cable during the operational phase.

In addition to the useful surface, it is possible to install a similar membrane on the opposite side in order to ensure the correct positioning of the elements and to avoid entanglement. In this case, the standard cable net could be used and the analytical model permits us to give a close approximation of the solution.

The problem of the network-membrane connection must also be solved from a technological point of view: transmission of forces, concentration of stresses and compliance with load limits.

A device to avoid the entanglement of the bars should be considered. A network that marries this with a shapely surface will also need to be studied.

Currently a prototype antenna with a network is being developed in the laboratory to perform static and dynamic tests using a gravity compensation device developed by Morterolle.

References:

[1] Tibert, Gunnar & Pellegrino, Sergio. (2002). Deployable Tensegrity Reflectors for Small Satellites. Journal of Spacecraft and Rockets. 39. 10.2514/2.3867.

[2] M.W. Thomson, The astromesh deployable reflector, Iutam-Iass Symposium on Deployable Structures: Theory and Applications 80 (2000) 435–446.

[3] J Quirant, F Cevaer, S Morterolle, B Maurin, JF Dubé. "Conceptual design and analysis of a deployable structure with flexible joints" - Journal of Aerospace Engineering, 2011.

[4] Thomson, M.W., "The AstroMesh deployable reflector,"Proc. Fifth International Mobile Satellite Conference (IMSC'97), 16-18 June 1997, Pasadena, CA, 1997, pp. 393-398. JPL Publication 97-11.

[5] Kellermeier, H., Vorbrugg, H., Pontoppidan, K., & Eaton, D. C. G. (1989). The ESA/MBB unfurlable mesh antenna development for mobile services. Acta Astronautica, 19(1), 47-56.

[6] Bettini, W., J. Quirant, J. Averseng and B. Maurin. 2018. "Self deployable geometries for space applications." J. Aerosp. Eng., 2019, 32 (1): DOI: 10.1061/(ASCE) AS.1943-5525.0000967.

[7] Sébastien Morterolle, Bernard Maurin, Jean-François Dube, Julien Averseng, Jérôme Quirant,

Modal behavior of a new large reflector conceptual design, Aerospace Science and Technology,

Volume 42, 2015, Pages 74-79, ISSN 1270-9638, https://doi.org/10.1016/j.ast.2015.01.002.

[8] Morterolle, S., B. Maurin, J. Quirant and C. Dupuy "Numerical form-finding of geotensoid tension truss for mesh reflector », Acta astronautica, Volume 76, July–August 2012, Pages 154-163 https://doi.org/10.1016/j.actaastro.2012.02.025.

[9] Tibert, G. (2003, April). Optimal design of tension truss antennas. In 44th AIAA/ASME/ASCE/AHS/ASC Structures, Structural Dynamics, and Materials Conference (p. 1629).

[10] Rodrigues Gonçalo, Angevain Jean-Christophe et Prowald Julian Santiago “Active shape control of reconfigurable antenna reflectors”, Proceedings of the 2nd International Conference "Advanced Lightweight Structures and Reflector Antennas". - 2014. - pp. 264-271.

[11] Santiago-Prowald, J., Baier, H. Advances in deployable structures and surfaces for large apertures in space. CEAS Space J 5, 89–115 (2013). https://doi.org/10.1007/s12567-013-0048-3

[12] Datashvili Leri “Dimensional stability and shape-accuracy of shell-membrane reflecting surfaces made of fibre-reinforced elastomers”, Proceedings of the 2nd International Conference "Advanced Lightweight Structures and Reflector Antennas". – 2014

[13] Juan Fayos, José Nieto, Álvaro Pipó Julián Santiago-Prowald, Tensegrity diaphanous dome demonstrator, 38th ESA Antenna Workshop on Innovative Antenna Systems and Technologies for Future Space Missions 3-6 October 2017, Noordwijk, The Netherlands.

[14] Juan Fayos, José Nieto, Álvaro Pipó Julián Santiago-Prowald, Large deployable reflectors based on tensegritic diaphanous domes, envisat symposium.

[15] Pellegrino S., Calladine C. R. Matrix analysis of statically and kinematically undeterminate frameworks, International Journal Solids and Structures, Vol 22-4, pp. 409-428, 1986.

[16] V. Raducanu, R. Motro *« Système à autoéquilibre stable pour élément de construction »*, Brevet d’invention déposé le 09/04/2001 aux noms de CNRS – Sté. Tissage et Enduction Serge Ferrari à l’INPI, enregistré sous le n°WO 02/08132 A1 à l’OMPI le 17/10/2002.

[17] Tserodz Sh. et al. New design of a transformable mechanical cone system with V-folding rods [Revue]// Proceedings of the 2nd International Conference "Advanced Lightweight Structures and Reflector Antennas".-2014.-pp. 89-98.

[18] Medzmariashvili-1 E. [et al.] Conical V-fold bar ring with flexible pre-stressed center, Proceedings of the 2nd International Conference "Advanced Lightweight Structures and Reflector Antennas".-2014.-pp. 391-399.

APPENDIX

APPENDIX A

Node 0: (A_1, S_0)

$$3A_1 \sin\alpha_1 + S_0 = 0 \tag{A.1}$$

Node 1': (A_1, B_2, S_1)

$$A_1 \cos\alpha_1 = 2B_2 \cos\beta_2 \cos\frac{\pi}{3} \tag{A.2}$$

$$A_1 \sin\alpha_1 + 2B_2 \sin\beta_2 + S_1 = 0 \tag{A.3}$$

Node 1: (B_1, A_2, S_1)

$$2B_1 \cos\beta_1 \cos\frac{\pi}{3} - A_2 \cos\alpha_2 = 0 \tag{A.4}$$

$$2B_1 \sin\beta_1 + A_2 \sin\alpha_2 + S_1 = 0 \tag{A.5}$$

Node 2: $(A_2, D_1, C_1 = 0, S_2)$

$$A_2 \cos\alpha_2 - D_1 \cos\delta_1 = 0 \tag{A.6}$$

$$A_2 \sin\alpha_2 + D1 \sin\delta_1 + S_2 = 0 \tag{A.7}$$

Node 2': (D_2, C_2, S_2)

$$2C_2 \cos\gamma_2 \cos\frac{\pi}{3} - D_2 \cos\delta_2 = 0 \tag{A.8}$$

$$2C_2 \sin\gamma_2 + D_2 \sin\delta_2 + S_2 = 0 \tag{A.9}$$

Node 3': (same that node 3) $(E_1, E_2, B_2, C_1 = 0, C_2, S_2)$

$$B_2 \cos\beta_2 \cos\frac{\pi}{6} - (E_1 + E_2)\cos\epsilon_1 \cos\psi = 0 \tag{A.10}$$

$$(E_2 - E_1)\cos\epsilon_1 \sin\psi - C_2 \cos\gamma_2 + B_2 \cos\beta_2 \sin\frac{\pi}{6} = 0 \tag{A.11}$$

$$B_2 \sin\beta_2 + (E_1 + E_2)\sin\epsilon_1 + C_2 \sin\gamma_2 + S_3 = 0 \tag{A.12}$$

Node 4: (E_1, E_2, D_1, D_2)

$$2(E_1 + E_2)\cos\epsilon_1 \cos\omega + (D_1 + D_2)\cos\delta_1 = T \tag{A.13}$$

Solving:

Node 0: (A_1, S_0)

$$A_1 = \underbrace{-\frac{1}{3\sin\alpha_1}}_{q_0} S_0 \qquad \text{(A.1')}$$

Injecting (A.1') in (2) and (3):

$$q_0 S_0 \cos\alpha_1 = 2B_2 \cos\beta_2 \cos\frac{\pi}{3} \qquad \text{(A.2')}$$

And,

$$q_0 S_0 \sin\alpha_1 + 2B_2 \sin\beta_2 + S_1 = 0 \qquad \text{(A.3')}$$

Leading to:

$$B_2 = \underbrace{\frac{1}{2}\frac{q_0 \cos\alpha_1}{\cos\beta_2 \cos\frac{\pi}{3}}}_{q_1} S_0 \qquad \text{(A.2'')}$$

By inserting (A.2) into (A.3):

$$S_1 = \underbrace{-(q_0 \sin\alpha_1 + 2q_1 \sin\beta_2)}_{q_2} S_0 \qquad \text{(A.3'')}$$

By injecting (A.3'') and (A.4) in (A.5):

$$B_1 = -\underbrace{\frac{q_2}{\left(2\sin\beta_1 + 2\cos\beta_1 \cos\frac{\pi}{3}\tan\alpha_2\right)}}_{q_3} S_0 \qquad \text{(A.5')}$$

Similarly, by putting (A.5') into (A.4):

$$A_2 = \underbrace{\frac{2q_3 \cos\beta_1 \cos\frac{\pi}{3}}{\cos\alpha_2}}_{q_4} S_0 \qquad \text{(A.4')}$$

By inserting (A.4') in (A.6):

$$D_1 = \underbrace{\frac{q_4 \cos\alpha_2}{\cos\delta_1}}_{q_5} S_0 \qquad \text{(A.6')}$$

$$A_2 \sin\alpha_2 + D1 \sin\delta_1 + S_2 = 0 \qquad \text{(A.7)}$$

By injecting (4') and (6') in (7):

$$S_2 = \underbrace{-(q_4 \sin\alpha_2 + q_5 \sin\delta_1)}_{q_6} S_0 \qquad \text{(A.7')}$$

$$D_2 = \underbrace{\frac{2\cos\gamma_2 \cos\frac{\pi}{3}}{\cos\delta_2}}_{q_7} C_2 \qquad \text{(A.8')}$$

By putting (A.7') and (A.8') in (A.9):

$$C_2 = -\underbrace{\frac{q_6}{2\sin\gamma_2 + q_7 \sin\delta_2}}_{q_8} S_0 \qquad \text{(A.9')}$$

This can be deduced by injecting (A.9) in (A.8'):

$$D_2 = \underbrace{q_7 q_8}_{q_9} S_0 \qquad \text{(A.8'')}$$

By injecting the relation (A.2') into equation (A.10), it comes:

$$E_1 + E_2 = \underbrace{\frac{q_1 \cos\beta_2 \cos\frac{\pi}{6}}{\cos\epsilon_1 \cos\psi}}_{q_{10}} S_0 \qquad \text{(A.10')}$$

By inserting (A.2'), (A.9') and (A.10') into (A.12):

$$S_3 = \underbrace{-(q_1 \sin\beta_2 + q_{10} \sin\epsilon_1 + q_8 \sin\gamma_2)}_{q_{11}} S_0 \qquad \text{(A.12')}$$

By putting (A.10') in (A.11):

$$2E_2 \cos\epsilon_1 \sin\psi = \left(q_{10} \cos\epsilon_1 \sin\psi + q_8 \cos\gamma_2 - q_1 \cos\beta_2 \sin\frac{\pi}{6}\right) S_0 \qquad \text{(A.11')}$$

$$E_2 = \underbrace{\frac{q_{10} \cos\epsilon_1 \sin\psi + q_8 \cos\gamma_2 - q_1 \cos\beta_2 \sin\frac{\pi}{6}}{2\cos\epsilon_1 \sin\psi}}_{q_{12}} S_0 \qquad \text{(A.11'')}$$

Injecting (A.11'') in (A.10'):

$$E_1 = (q_{10} - q_{12}) S_0 \qquad \text{(A.10'')}$$

Finally, injecting (A.6'), (A.8') and (A.10') in (A.13):

$$S_0 = \frac{T}{2q_{10}\cos\epsilon_1 \cos\omega + (q_5 + q_9)\cos\delta_1} \qquad \text{(A.13')}$$

So, finally:

$$S_0 = \frac{T}{q_{13}} \qquad \text{(A.13'')}$$

T is the enter parameter, S_0 is known, the other parameters are deduced in function of T. Parameters are listed in Table A.1.

Standard Network parameters	
$q_0 = -\frac{1}{3\sin\alpha_1}$	$q_7 = \frac{2\cos\gamma_2\cos\frac{\pi}{3}}{\cos\delta_2}$
$q_1 = \frac{\frac{1}{2}q_0\cos\alpha_1}{\cos\beta_2\cos\frac{\pi}{3}}$	$q_8 = -\frac{q_6}{2\sin\gamma_2 + q_7\sin\delta_2}$
$q_2 = -(q_0\sin\alpha_1 + 2q_1\sin\beta_2)$	$q_9 = q_7 q_8$
$q_3 = -\frac{q_2}{2\sin\beta_1 + 2\cos\beta_1\cos\frac{\pi}{3}\tan\alpha_2}$	$q_{10} = \frac{q_1\cos\beta_2\cos\frac{\pi}{6}}{\cos\epsilon_1\cos\psi}$
$q_4 = \frac{2q_3\cos\beta_1\cos\frac{\pi}{3}}{\cos\alpha_2}$	$q_{11} = -(q_1\sin\beta_2 + q_{10}\sin\epsilon_1 + q_8\sin\gamma_2)$
$q_5 = \frac{q_4\cos\alpha_2}{\cos\alpha_1}$	$q_{12} = \frac{q_{10}\cos\epsilon_1\sin\psi + q_8\cos\gamma_2 - q_1\cos\beta_2\sin\frac{\pi}{6}}{2\cos\epsilon_1\sin\psi}$
$q_6 = -(q_4\sin\alpha_2 + q_5\sin\delta_1)$	$q_{13} = 2q_{10}\cos\epsilon_1\cos\omega + (q_5 + q_9)\cos\delta_1$

Tab. A.1. Standard Network parameters

APPENDIX B

Given that $N_i(X) = M_i X + P_i$:

$$\sum_{i=1}^{n} \frac{1}{E_i S_i} \int_0^{\ell_i} M_i^2 X + M_i P_i \, dy = 0 \tag{B.1}$$

$$\sum_{i=1}^{n} \frac{\left(M_i^2 X + M_i P_i\right)\ell_i}{E_i S_i} = 0 \tag{B.2}$$

$$X \sum_{i=1}^{n} \frac{M_i^2 \ell_i}{E_i S_i} + \sum_{i=1}^{n} \frac{M_i P_i \ell_i}{E_i S_i} = 0 \tag{B.3}$$

$$X = -\frac{\sum_{i=1}^{n} \frac{M_i P_i \ell_i}{E_i S_i}}{\sum_{i=1}^{n} \frac{M_i^2 \ell_i}{E_i S_i}} \tag{B.4}$$

The modified equations of the reinforced cable net are denoted with (*):

$$A_2 \cos\alpha_2 - D_1 \cos\delta_1 + 2C_1 \cos\gamma_1 \cos\chi = 0 \tag{B.6*}$$

$$A_2 \sin\alpha_2 + D_1 \sin\delta_1 + 2C_1 \sin\gamma_1 + S_2 = 0 \tag{B.7*}$$

$$(E_2 - E_1)\cos\epsilon_1 \sin\psi - C_2 \cos\gamma_2 + B_2 \cos\beta_2 \sin\frac{\pi}{6} - C_1 \cos\gamma_1 = 0 \tag{B.11*}$$

$$B_2 \sin\beta_2 + (E_1 + E_2)\sin\epsilon_1 + C_2 \sin\gamma_2 + S_3 - C_1 \sin\gamma_1 = 0 \tag{B.12*}$$

The equations are wrote in function of $C_1 = X$ and listed in Table B.1 and coefficients are listed in Table B.2.

Normal force	Derivative following X
Bars	
$S_0 = \frac{T}{\lambda_{11}} - \frac{\lambda_{12}}{\lambda_{11}} X$	$\frac{\partial S_0}{\partial X} = \frac{-\lambda_{12}}{\lambda_{11}}$
$S_1 = q_2 \frac{T}{\lambda_{11}} - q_2 \frac{\lambda_{12}}{\lambda_{11}} X$	$\frac{\partial S_1}{\partial X} = q_2 \frac{-\lambda_{12}}{\lambda_{11}}$
$S_2 = \lambda_0 \frac{T}{\lambda_{11}} + \left(\lambda_0 \frac{-\lambda_{12}}{\lambda_{11}} + \lambda_1\right) X$	$\frac{\partial S_2}{\partial X} = \lambda_0 \frac{-\lambda_{12}}{\lambda_{11}} + \lambda_1$
$S_3 = \lambda_5 \frac{T}{\lambda_{11}} + \left(\lambda_5 \frac{-\lambda_{12}}{\lambda_{11}} + \lambda_6\right) X$	$\frac{\partial S_3}{\partial X} = \lambda_5 \frac{-\lambda_{12}}{\lambda_{11}} + \lambda_6$
Cables	
$A_1 = q_0 \frac{T}{\lambda_{11}} - q_0 \frac{\lambda_{12}}{\lambda_{11}} X$	$\frac{\partial A_1}{\partial X} = q_0 \frac{-\lambda_{12}}{\lambda_{11}}$
$A_2 = q_4 \frac{T}{\lambda_{11}} - q_4 \frac{\lambda_{12}}{\lambda_{11}} X$	$\frac{\partial A_2}{\partial X} = q_4 \frac{-\lambda_{12}}{\lambda_{11}}$
$B_1 = q_3 \frac{T}{\lambda_{11}} - q_3 \frac{\lambda_{12}}{\lambda_{11}} X$	$\frac{\partial B_1}{\partial X} = q_3 \frac{-\lambda_{12}}{\lambda_{11}}$
$B_2 = q_1 \frac{T}{\lambda_{11}} - q_1 \frac{\lambda_{12}}{\lambda_{11}} X$	$\frac{\partial B_2}{\partial X} = q_1 \frac{-\lambda_{12}}{\lambda_{11}}$
$C_1 = X$	$\frac{\partial C_1}{\partial X} = 1$
$C_2 = \lambda_2 \frac{T}{\lambda_{11}} + \left(\lambda_3 - \lambda_2 \frac{\lambda_{12}}{\lambda_{11}}\right) X$	$\frac{\partial C_2}{\partial X} = \lambda_2 \frac{-\lambda_{12}}{\lambda_{11}} + \lambda_3$
$D_1 = \eta \frac{T}{\lambda_{11}} + \left(\mu - \eta \frac{\lambda_{12}}{\lambda_{11}}\right) X$	$\frac{\partial D_1}{\partial X} = \mu + \eta \frac{-\lambda_{12}}{\lambda_{11}}$
$D_2 = q_7 \lambda_2 \frac{T}{\lambda_{11}} + q_7 \left(\lambda_3 - \lambda_2 \frac{\lambda_{12}}{\lambda_{11}}\right) X$	$\frac{\partial D_2}{\partial X} = q_7 \left(\lambda_2 \frac{-\lambda_{12}}{\lambda_{11}} + \lambda_3\right)$
$E_1 = (\lambda_4 - \lambda_7) \frac{T}{\lambda_{11}} - \left((\lambda_4 - \lambda_7) \frac{\lambda_{12}}{\lambda_{11}} + \lambda_8\right) X$	$\frac{\partial E_1}{\partial X} = (\lambda_4 - \lambda_7) \frac{-\lambda_{12}}{\lambda_{11}} - \lambda_8$
$E_2 = \lambda_7 \frac{T}{\lambda_{11}} + \left(-\lambda_7 \frac{\lambda_{12}}{\lambda_{11}} + \lambda_8\right) X$	$\frac{\partial E_2}{\partial X} = \lambda_7 \frac{-\lambda_{12}}{\lambda_{11}} + \lambda_8$

Tab.B.1 Representation of the normal force in function of the geometrical coefficients

Reinforced network	
$\mu = \frac{2\cos\gamma_1 \cos\frac{\pi}{3}}{\cos\gamma_1}$	$\lambda_6 = -(\lambda_3 \sin\gamma_2 - \sin\gamma_1)$
$\eta = \frac{q_4 \cos\alpha_2}{\cos\delta_1}$	$\lambda_7 = -\frac{-\lambda_4 \cos\epsilon_1 \sin\psi - \lambda_2 \cos\gamma_2 + q_1 \cos\beta_2 \sin\frac{\pi}{6}}{2\cos\epsilon_1 \sin\psi}$
$\lambda_0 = -q_4(\sin\alpha_2 - \cos\alpha_2 \tan\delta_1)$	$\lambda_8 = \frac{\cos\gamma_1 + \lambda_3 \cos\gamma_2}{2\cos\epsilon_1 \sin\psi}$
$\lambda_1 = \frac{2\cos\gamma_1 \cos\frac{\pi}{3}}{\cos\delta_1}\sin\delta_1 - 2\sin\gamma_1$	$\lambda_9 = -\frac{2\cos\gamma_1 \cos\frac{\pi}{3}}{\cos\delta_1}$
$\lambda_2 = -\frac{\lambda_0}{2\sin\gamma_2 + q_7 \sin\delta_2}$	$\lambda_{10} = -\frac{q_4 \cos\alpha_2}{\cos\delta_1}$
$\lambda_3 = -\frac{\lambda_1}{2\sin\gamma_2 + q_7 \sin\delta_2}$	$\lambda_{11} = 2\lambda_4 \cos\epsilon_1 \cos\omega + \lambda_{10} \cos\delta_1 + q_7\lambda_2 \cos\delta_1$
$\lambda_4 = \frac{q_1 \cos\beta_2 \cos\frac{\pi}{6}}{\cos\epsilon_1 \cos\psi}$	$\lambda_{12} = (\lambda_9 + q_7\lambda_3)\cos\delta_1$
$\lambda_5 = -(\lambda_4 \sin\epsilon_1 + \lambda_2 \sin\gamma_2 + q_1 \sin\beta_2)$	

Tab.B.2. Representation of different geometrical parameters